# Development and Investigation of Cone-Type Five-Hole Probes for Small Gas Turbines

W. Koschel and P. Pretzsch

March 1988

Abstract

Development and Investigation of Cone-Type Five-Hole Probes for Small Gas Turbines

The presentation is concerned to the development of miniaturized multi-hole probes for application in transonic axial turbines with small blade heights. The calibration method which is based on the multi-parameter approximation in flow angles and Mach numbers is shortly described.

Probe calibration is carried out in a closed-loop wind tunnel allowing to investigate the probes at different subsonic and supersonic Mach numbers in a wide range of Reynolds numbers. For the calibration well-tested measurement techniques are used with fully automated data acquisition and subsequent evaluation by means of large-scale computers.

During the probe development special attention had been given to the effects due to shock interactions between shaft and probe head. Different configurations of cone-type probe dummies with varying shaft cross sections and head geometries had been tested in a wide range of transonic Mach numbers. The shock interference could be studied by visualization using Schlieren photography.

In addition some experimental results of investigations concerning aerodynamic effects like sidewall-probe interaction and the influence of the Reynolds number on the characteristic calibration parameters are presented and discussed.

Contents



## 1. Introduction

The experimental investigation of modern turbine stages with high power capacity requires the availability of high-quality measuring equipment. Especially the measuring of transonic turbines expects a great deal from the instrumentation of the test bench. So there are only few alternatives in measuring the turbine flow concerning pressure, velocity and direction. Pneumatic pressure probes are used with preference in stationary measurements.

The Institut of Jet Propulsion and Turbomachinery (Technical University of Aachen, Germany) has experiences of long standing in the sphere of multihole-probe measuring techniques. The submitted documentation describes the state of art in fully automated pressure probe calibration. The turbine stages which are investigated in the institute have rather small flow channel dimensions, so that adequately miniaturized pressure probes are required. The hitherto available types have been permanently advanced and adapted to new requirements. So the development of such a new probe type and the following investigation of the resulting probe features are shown afterwards.

## 2. Symbols

| | |
|---|---|
| $C_{i,j,k}$ | coefficients |
| H | channel height |
| $K_\alpha$ | characteristic quantity for the angle $\alpha$ |
| $K_\beta$ | characteristic quantity for the angle ß |
| $K_M$ | characteristic quantity for the Mach number |
| $K_T$ | characteristic quantity for the total pressure |
| $K_S$ | characteristic quantity for the static pressure |
| L,M,N | polynomial degrees |
| M | Mach number |
| $p_i$ | probe pressures (i = 0,1,2,3,4) |
| p | static pressure |
| $p_t$ | total pressure |
| Re | Reynolds number |
| $U_i$ | voltage signals of the CEC-sensor (i = 0,1,2,3,4) |
| X1,X2,X3 | characteristic quantities of the polynomial equation |
| Y | approximated flow quantity |
| $\alpha$ | yaw angle |
| ß | pitch angle |
| $\delta$ | head cone angle |

## 3. Calibration of Pneumatic Pressure Probes

### 3.1 Definition of the Characteristic Quantities

Pneumatic pressure probes (multi-hole-probes) are mainly used for the inquiry of the total pressure, the Mach number and the flow direction. In the case of a five-hole-probe it is possible to find out the spacial flow vector. For the effective calibration and the subsequent application of the probe it is necessary to formulate mathematical relations in order to combine the five measured pressures and the requested flow quantities. Therefore clear definitions of the yaw angle $\alpha$ and the pitch angle ß have to be fixed, which are illustrated in fig. 1. Moreover the pressure bore holes of the probe can be provided with index numbers, so that the following characteristic quantities are deduced:

- for the yaw angle

$$K_\alpha = \frac{p_3 - p_1}{\Delta p}$$

- for the pitch angle

$$K_\beta = \frac{p_4 - p_2}{\Delta p}$$

- for the Mach number

$$K_M = \frac{\Delta p}{p_0}$$

- for the total pressure

$$K_T = \frac{p_t - p_0}{\Delta p}$$

- for the static pressure

$$K_S = \frac{p_0 - p}{\Delta p}$$

with $$\Delta p = p_0 - \frac{p_1 + p_3}{2}$$

In these equations the indexing corresponds to the bore hole numbers.

Moreover means:

$p_t$ : total pressure of the calibration flow
$p$ : static pressure of the calibration flow

With knowledge of these characteristic quantities from the calibration of the concerning probe and with the results of the evaluation described as follows it is possible to acquire the flow quantities $\alpha$, ß and M by the five pressure signals of such a probe directly. For the calculation of the total pressure and the static pressure the following equations are valid:

$$p_t = p_0 + K_T \cdot \Delta p$$

$$p = p_0 - K_S \cdot \Delta p$$

## 3.2 Approximation Polynom and Probe Coefficients

The notation of the flow quantity Y, which is to be approximated (Y = $\alpha$, ß, M, $K_T$, $K_S$), as function of the three independent non-dimensional characteristic quantities X1 (X1 = $K_\alpha$), X2 (X2 = $K_ß$) and X3 (X3 = $K_M$) can be done by formulating a polynomial equation for a five-hole probe as follows:

$$Y = \sum_{i=1}^{L} \left[ \sum_{j=1}^{M} \left[ \sum_{k=1}^{N} C_{ijk} X3^{k-1} \right] X2^{j-1} \right] X1^{i-1}$$

$$\begin{aligned}
&= [\,[\,C_{111} + C_{112}X3 + C_{113}X3^2 + \ldots + C_{11N}X3^{N-1}] + \\
&\quad + [\,C_{121} + C_{122}X3 + C_{123}X3^2 + \ldots + C_{12N}X3^{N-1}]\,X2 + \\
&\quad + [\,C_{131} + C_{132}X3 + C_{133}X3^2 + \ldots + C_{13N}X3^{N-1}]\,X2^2 + \\
&\quad \ldots \\
&\quad + [\,C_{1M1} + C_{1M2}X3 + C_{1M3}X3^2 + \ldots + C_{1MN}X3^{N-1}]\,X2^{M-1}] + \\
&+ [\,[\,C_{211} + C_{212}X3 + C_{213}X3^2 + \ldots + C_{21N}X3^{N-1}] + \\
&\quad + [\,C_{221} + C_{222}X3 + C_{223}X3^2 + \ldots + C_{22N}X3^{N-1}]\,X2 + \\
&\quad + [\,C_{231} + C_{232}X3 + C_{233}X3^2 + \ldots + C_{23N}X3^{N-1}]\,X2^2 + \\
&\quad \ldots \\
&\quad + [\,C_{2M1} + C_{2M2}X3 + C_{2M3}X3^2 + \ldots + C_{2MN}X3^{N-1}]\,X2^{M-1}]\,X1 + \\
&+ [\,[\,C_{311} + C_{312}X3 + C_{313}X3^2 + \ldots + C_{31N}X3^{N-1}] + \\
&\quad + [\,C_{321} + C_{322}X3 + C_{323}X3^2 + \ldots + C_{32N}X3^{N-1}]\,X2 + \\
&\quad + [\,C_{331} + C_{332}X3 + C_{333}X3^2 \quad + C_{33N}X3^{N-1}]\,X2^2 + \\
&\quad \ldots \\
&\quad + [\,C_{3M1} + C_{3M2}X3 + C_{3M3}X3^2 \quad + C_{3MN}X3^{N-1}]\,X2^{M-1}]\,X1^2 + \\
&\quad \ldots \\
&+ [\,[\,C_{L11} + C_{L12}X3 + C_{L13}X3^2 + \ldots + C_{L1N}X3^{N-1}] + \\
&\quad + [\,C_{L21} + C_{L22}X3 + C_{L23}X3^2 + \ldots + C_{L2N}X3^{N-1}]\,X2 + \\
&\quad + [\,C_{L31} + C_{L32}X3 + C_{L33}X3^2 + \ldots + C_{L3N}X3^{N-1}]\,X2^2 + \\
&\quad \ldots \\
&\quad + [\,C_{LM1} + C_{LM2}X3 + C_{LM3}X3^2 + \ldots + C_{LMN}X3^{N-1}]\,X2^{M-1}]\,X1^{L-1}
\end{aligned}$$

Out of that the coefficients $C_{i,j,k}$ for every flow quantity, which is to be approximated, will result with a compensating calculation (curve fitting) according to the least square method. The polynomial degrees (L-1), (M-1) and (N-1) are varied in more than one computer job during the evaluation, until the optimal approximation polynom has been found. The criterion for the optimal solution is on the one hand to minimize the maximum and the mean error, on the other hand to avoid an oscillating solution.

It is quite difficult to stabilize transonic Mach numbers (here: $0.93 < M < 1.17$) in the closed tunnel of the institute during a probe calibration, therefore approximation inaccuracies have to be expected in this range of Mach number. So three separate approximative calculations are accomplished with different distribution of coefficients in each case in agreement with the number of calibration points. One approximation covers the whole calibration range including the transonic range without any calibration point and so later on evaluations of measurements are possible in the whole range of Mach number. However this approximation will result in considerable mean errors in comparison because of the fact described before. Two other approximations include in each case the subsonic and supersonic range separately and result in essentially more convenient mean errors. All these approximations produce quite high errors in extrapolation, and therefore the level of the Mach number of the measuring

flow has to be known in using the coefficients of a separate approximation so that the measuring points lie within the approximated range of Mach number.

### 3.3 Investigation Procedure and Data Acquisition

The calibrations of transonic pressure probes are carried out in the closed calibration tunnel of the institute (fig. 2 and fig. 3). The adjustment of the Mach number of the calibration flow for the different calibration points is executed with the speed of the supplying compressor in the subsonic range, and for the supersonic range interchangeable Laval nozzles are available for the Mach numbers $M \geq 1.2$.

Before the calibration starts the probe is equalized aerodynamically ($p_1 = p_3$). During the calibration the angles $\alpha$ and $\beta$ are varied by yawing and pitching the probe for each adjusted Mach number. The corresponding probe support is shown in assembled condition in fig.3. The adjustment of the probe position in $\alpha$- and $\beta$-direction and the acquisition of motor positions, pressure measurement values and the channel total temperature is performed with an in-process computer LSI 11/23 by usage of adequate periphery (fig. 4). The corresponding connection scheme is shown in fig. 5. The calibration procedure is fully automated expect the adjustment of the channel Mach number and lasts about 35 minutes for one Mach number and 99 calibration points.

The evaluation of the pressure quantities acquired by the in-process computer, the calculation of the charcteristic probe quantities, the subsequent approximation and error inquiry are performed with a large-scale computer CYBER 170-825.

## 4. Development of a New Probe Type

### 4.1 Targets and Requirements

This chapter describes the latest development of a cone-type five-hole probe for the application in the test bench of a transonic high pressure turbine stage. The desired features of the probe were in detail:

- little blockage of the measuring channel
- few shock interactions between probe shaft and head
- high sensitivity for $\alpha$ and $\beta$ measurement
- adjacent shock at the probe head and high recovery of total pressure
- unsensitivity of total pressure with $\alpha$ in a range of $-10^0 < \alpha < 10^0$

Because of the lack of space in the concerning machine the probe should be inserted through a hole of $\emptyset = 14$ mm with practicable radial traversing. The shaft tube should have an outer diameter

of 10 mm, and the section of the shaft exposed to the flow should be as small as possible for little blockage. For the layout of the probe head cone angle two contrary demands had to be agreed upon. A small cone angle is desirable for gasdynamic reasons. With that the head shock will be adjacent in a wide range of Mach number, for example the shock is adjacent with the head angle $\delta = 30^0$ at $M = 1.12$, whereas with the head angle $\delta = 45^0$ a Mach number of $M = 1.27$ is necessary for that. Small cone angles have certainly one disadvantage. The five pressure bore holes of the probe head should be situated close together to minimize the geometric deviation between the particular bore holes and the spot of measurement. For the chosen head diameter of 2.7 mm the circle, which contains the bore holes 1-4, has a diameter of 1.68 mm by manufacturing demands. The different positions for the lateral bore holes as function of the cone angle are shown in fig. 6 for the suitable range. The two other main geometric construction features are the head length, which should be in the range of 9 to 13.8 mm, and the cross-section profile of the shaft part, which is exposed to the flow. The leading region should be wedge-shaped for an adjacent shock. But there has also to be enough space for the five pressure tubes. So the different boundary conditions have been fixed for the subsequently described construction of the probe type.

## 4.2 Investigation of Different Design Principles

The interesting design types of the pneumatic pressure probes described herein were firstly manufactured out of full material (so-called dummies) with identical outer dimensions. At that two different shaft cross-sections and diverse head cone angles had been chosen. One cross-section design ("A", fig. 7) had a drop-like geometry with very sharp leading edge and following continuous widening of the cross-section up to the maximum breadth of the shaft (2.7 mm). The small wedge angle at the leading edge in combination with the continuous widening of the cross-section should cause the shaft shock to be adjacent and should avoid another oblique shock at a perhaps discontinuous widening. Moreover convenient performance had to be expected concerning the flow separation in subsonic application and the extent of the dead water region. This shaft design promises aerodynamic advantages, but it causes extreme expenditure in manufacturing. In addition the exact profile cannot be guaranteed with the available practicabilities of manual work. Therefore a second profile design was created alternatively with a simple geometry ("B"). The rather large wedge angle of $\delta/2 = 27.5^0$ is suspicious. With that an adjacent shaft shock is not possible, because the maximum angles are $\delta/2 = 4^0$ with $M = 1.2$ and $\delta/2 = 9.25^0$ with $M = 1.4$.

Another main design aspect is the question of shaft crimping. Collectively four shaft versions (dummies) with different geometries and cross-sections were manufactured for the subsequent

investigations (fig. 8). Every shaft could be equipped with heads of different length and cone angle (30°,35°,45°) (fig. 9).

The investigation of the flow around the shaft and the head of the dummies with different Mach numbers and adjusted angles was carried out with a Schlieren photography equipment at the closed calibration tunnel of the institute (fig. 10). The following fundamental questions should be answered:

1. Are the aerodynamic advantages of the drop-design so significant, that the higher fabrication expenditure compared to the prismatic design will be profitable?
2. Which influence does the design of the shaft crimping have upon the shaft shock and the shock interaction?
3. How does the variation of the probe head length alter the shock configuration at the probe head?

The fig. 11a-d show that the shock is situated in front of the shaft with M = 1.17 for both configurations; at this level of Mach number the drop-design has no obvious advantage in comparison with the prismatic one. But also with M = 1.4 there is no appreciable difference in the position of the shaft shock. The cross-section area, which is necessary for the function (pressure tubes) and the stability of the probe, is too large to achieve an adjacent shock at the sharp leading edge of the shaft. Otherwise the constructive restrictions concerning the shaft cross-section are rather fixed, so that on principle another contour cannot be realized. From there in this case the prismatic design will be prefered and not the drop-design.

The influence of different shaft crimping is shown in fig. 12a,b. Clear differences in the flow structure result firstly with higher Mach numbers (M = 1.4). With the large crimping the separated shaft shock and the adjacent head shock can be differentiated, with the small crimping there is a unique shock in front of the probe. A second shock is visible at the shaft bend, which is situated just through the region of the bore holes. Such an effect is disadvantageous, because the results of a calibration will have to be called in question, if the position of those additional shocks and the flow field (i.e. due to instable transonic Mach numbers) are not reproducible. In this case the use of straight shafts should be taken into account. This aspect was investigated by two dummies with prismatic design and equal heads. For the flow Mach number M = 1.4 there is no appreciable difference in the flow field around the head (fig. 14a,b), in both cases the head shocks are adjacent. Certainly the shaft shock of the crimped version is placed farther in front of the shaft than for the straight one, so that the shock configuration resulting from the shock interaction is closer to the probe head for the crimped design. Distinct advantages are visible for the straight shaft at M = 1.17. In the case of the crimped shaft the shock is clearly in front of the dummy for both angle positions ($\beta = +15°$, $\beta = -15°$), so that the head flow is always influenced by the shaft. For the straight shaft this effect can

only be seen for $\beta = +15^0$, else the head shock is not influenced by the shaft shock for smaller values of angle $\beta$. The straight shaft has the advantage that the shaft shock does not have to follow the crimped contour and so it is situated behind the head cone for lower Mach numbers, too. Considering the fabrication expenditure the straight design is quite better, because there are several material separations and at least one soldering joint less. So also errors concerning the solidity and the closeness will be avoided.

There is no effect of the probe head length in the transonic range (M = 1.17), but in the case of M = 1.4 an adjacent shock is visible at the long head, whereas the tip of the short head is just behind the shaft shock (fig. 13a,b). With regard to the constructive aspect of the head length it is additionally necessary to consider that the shaft dams up the subsonic flow in the region of the bore hole "4" and so the resolution and exactness may be unfavourably influenced for large $\beta$-angles. Therefore the head length should be as long as possible with the restriction of the minimized distance between the region of the bore holes and the probe axis, so that the extent of the measuring point is limited to the bore hole distance and will not be an arc of a circle while turning the probe.

Finally the question of the size of the head cone angle will be dealt with. Therefore the straight shaft had been equipped with heads of the same length with different cone angles. There was no visible advantage for any cone angle at M = 1.4. The Mach number M = 1.17 causes on the contrary adjacent shocks for the angles $30^0$ and $35^0$, all the separation starts to be visible at $45^0$ (fig. 16a,b). The differences between the two small angles concerning the flow are negligible and so the angle should be $35^0$ considering the problem of bore hole distances.

## 4.3 Construction and Fabrication of the Probe

The preceding investigations resulted in the following constructive boundary conditions to be an acceptable compromise between aerodynamic quality, low expenditure in fabrication and well-conceived functionality:

- straight and backward situated shaft,
- prismatic shaft design,
- maximum head length of 13.4 mm
- head cone angle $\delta = 35^0$

So the probe was created like it is shown in fig. 17. The fabrication of the prototype and the first small-lot with different modifications was carried out by manual work in the workshop of the institute (fig. 18). The first results are shown in fig. 19 for application in transonic turbines with different blade heights. All parts are made with high-alloy-steel and all part connections are hard-soldered.

## 5. Investigations of the New Probe Type

### 5.1 Results of the Calibration

The calibration of the probes was done with the following calibration points:

$\alpha$: $-15^0$, $-12^0$, $-9^0$, $-6^0$, $-3^0$, $0^0$, $3^0$, $6^0$, $9^0$, $12^0$, $15^0$
$\beta$: $-5^0$, $-3^0$, $-1^0$, $0^0$, $1^0$, $3^0$, $5^0$, $7^0$, $10^0$,
M: 0.4, 0.5, 0.6, 0.7, 0.81, 0.92, 1.2, 1.3, 1.37, 1.5

With the ten different Mach numbers the tunnel flow had the following Reynolds numbers related to the head diameter as characteristic length:

| M | 0.4 | 0.5 | 0.6 | 0.7 | 0.81 | 0.92 |
|---|---|---|---|---|---|---|
| $Re \cdot 10^{-5}$ | 0.23 | 0.288 | 0.331 | 0.368 | 0.398 | 0.426 |

| M | 1.2 | 1.3 | 1.37 | 1.5 |
|---|---|---|---|---|
| $Re \cdot 10^{-5}$ | 0.462 | 0.466 | 0.491 | 0.498 |

The results of the calibration are illustrated in the manner $K_\beta = f(K_\alpha)$ with the parameters $\alpha$ and $\beta$ for a constant Mach number. Such a calibration map is exemplary shown in fig. 20 for a subsonic Mach number.

With consideration of the geometry the probe has a good sensitivity in $\alpha$-measurement and an acceptable symmetry around the balanced position ($\alpha = 0^0$). The shaft influence, that is the damming-up effect is rather small ($|K_\beta|_0 = f(\beta = 0^0)$). The slight asymmetrie of the maps for large positive values of $\beta$ and large amounts of $\alpha$ can be explained by tolerances in fabrication, but these effects are included in the approximative calculation. The total pressure resolution has very good results in the range of $-12^0 < \alpha < 12^0$; for extreme $\beta$-values this range is restricted to $-9^0 < \alpha < 9^0$. The calibration points of the Mach number M = 1.2 are insignificantly scattered, because the adjustment of a stable working point is problematic in this range. Moreover the earlier described shock effects appear with this Mach number, which influence the symmetry of the calibration map (fig.21). The approximation of the characteristic probe quantities to calculate the calibration coefficients was made under use of the procedure described in chapter 3.2. The following mean errors resulted in three separate calculations:

1. approximation of all points of calibration
2. separate approximation of all subsonic points
3. separate approximation of all supersonic points

| | | 1 | 2 | 3 |
|---|---|---|---|---|
| $\Delta\alpha$ | [deg] | 0.1677 | 0.0758 | 0.0945 |
| $\Delta\beta$ | [deg] | 0.1794 | 0.0875 | 0.2526 |
| $\Delta M$ | [-] | 0.0303 | 0.0107 | 0.0246 |

| | | | |
|---|---|---|---|
| $\Delta K_T$ [-] | 0.0162 | 0.0017 | 0.0352 |
| $\Delta K_S$ [-] | 0.0383 | 0.0177 | 0.0126 |

The unfavourable influence of the existence and the interaction of head and shaft shocks is represented by the rather high mean errors for the angle ß in supersonic range of Mach number.

## 5.2 Influence of the Reynolds Number

After the calibration the static pressure level in the calibration tunnel was varied for two chosen points in order to investigate the influence of different Reynolds numbers on the characteristic probe quantities:

M = 0.7 $Re_1 = 0.366 \cdot 10^5$
$Re_2 = 0.583 \cdot 10^5$
$Re_3 = 0.816 \cdot 10^5$

M = 1.2 $Re_1 = 0.516 \cdot 10^5$
$Re_2 = 0.714 \cdot 10^5$
$Re_3 = 0.925 \cdot 10^5$

The results of this investigation show that there are only very small fluctuations in $K_\alpha = f(\alpha, Re)$ in the range of $|\alpha| < 10^0$ (fig. 22a), especially under consideration of the fact that the Reynolds number had to be adjusted for each Mach number separately which caused little deviations, too. There are insignificantly larger deviations for the quantity $K_\beta = f(\beta, Re)$ (fig. 22b) because of the shaft effect in subsonic flow (damming-up effect), just as for $K_S = f(\beta, Re)$. The characteristic quantities $K_M$ and $K_T$ versus $\alpha$ are nearly independent of the Reynolds number. Comprehensively pointed out, no appreciable differences in probe performance could be found concerning the Reynolds number in the investigated range. Hence after the calibration in a fixed Reynolds number level the probe may be used in different flow conditions with other Reynolds numbers without essential loss in accuracy and resolution.

## 5.3 Wall Influence

The probe will be applicated in comparatively small flow channels, so the investigation of the probe signals near a wall was interesting. To that purpose the probe was traversed about the calibration tunnel height for $\alpha = 0^0$ and $\beta = 0^0$. The illustrations fig. 23a-c show the characteristic quantities $K_\alpha$, $K_\beta$ and $K_M$ versus the tunnel height in the upper diagram; the voltage signals of the CEC-sensor are shown in the lower diagram with offset voltage rejection. In subsonic flow there is a pressure signal decrease in the near of the wall caused by the boundary layer and the nozzle effect between the probe head and the wall. With approaching to the upper wall there are also boundary layer and acceleration effects and a anomalous curve of

the $K_\beta$-quantity, which might result to wrong evaluation of the pitch angle applied to the normal wide-channel calibration, if the probe is used near a wall. In the supersonic case it is unfortunately not possible to realize a constant Mach number for the whole tunnel height, so that $K_M$ decreases considerably. The curves of $K_\alpha$ in subsonic and supersonic flow have a slight variation versus tunnel height, which can be explained by a twist in the tunnel flow. The variation of the $K_\beta$-quantity in supersonic flow is evidently caused by the approach to the wall, but also boundary layer and shock effects will be important. The investigation of the probe signals with approach to an upper wall in supersonic flow was not yet possible.

## 6. Summary

This documentation describes the particular steps of development of a pneumatic pressure probe with regard to aerodynamic quality, low expenditure in fabrication and reasonable application. The procedure of a probe calibration is illustrated and some results are presented for the new probe type. The performance of the probe is proved, also the efficiency concerning the level of the Reynolds number and the wall influence.

More theoretical investigations of the flow around the probe head are planned and will deal with the problems of wall influence and shaft influence on the probe head to verify the sum of different effects with experimental results in order to find useful correction methods.

## 7. Bibliography

D. Bohn, H. Simon
Mehrparametrige Approximation der Eichräume und Eichflächen von Unterschall- bzw. Überschall-Fünf-Loch-Sonden
ATM, Meßtechnische Praxis
März 1975, Lieferung 470

K.-D. Broichhausen, G. Kauke
Übertragbarkeit der Kalibrierung von Sonden für verschiedene Reynoldszahlen in Unter- und Überschallströmungen
Mitteilung Nr. 81-08
Institut für Strahlantriebe und Turboarbeitsmaschinen
RWTH Aachen, Oktober 1981

L. A. Vasiliev
Schlierenmethods
Israel Program for Scientific Translations
New-York, Jerusalem, London 1971

H. Zebner
Procedure and Computer Program for the Approximation of Data
Monterey 1980, NPS67-80-001 CR

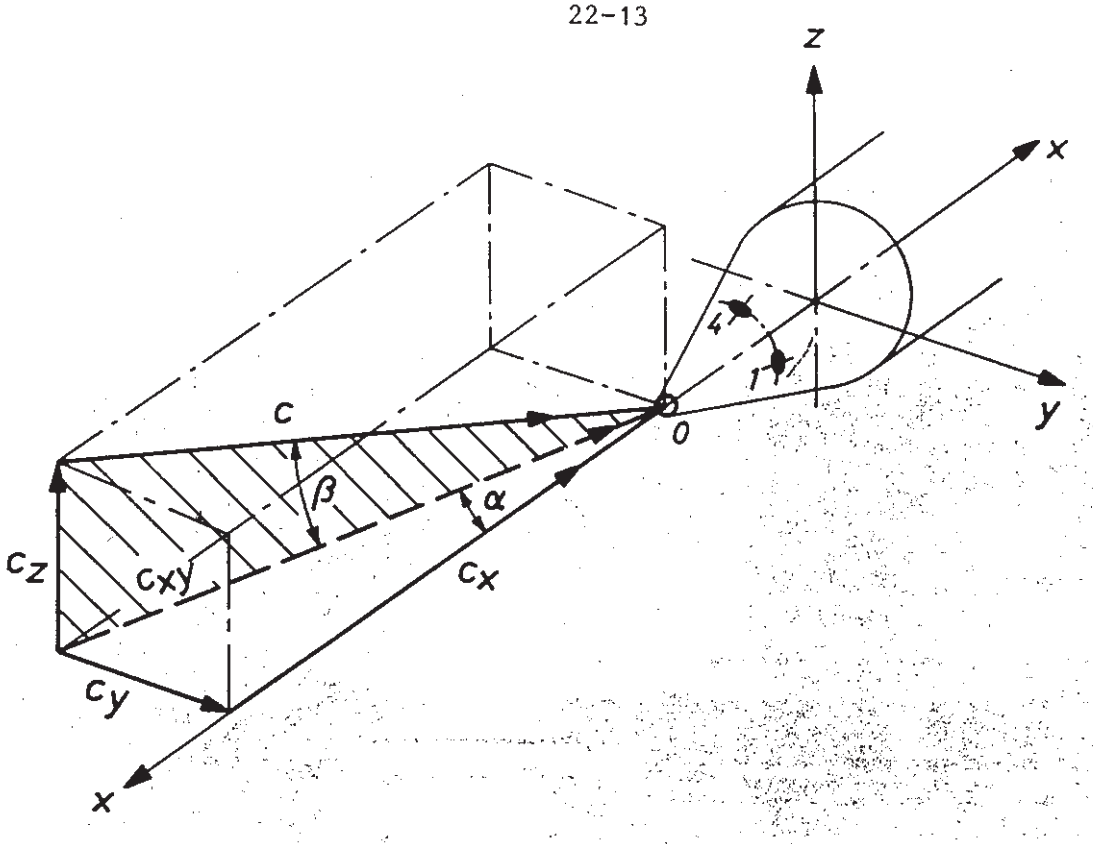


Fig. 1 Bore holes and angles at the probe head

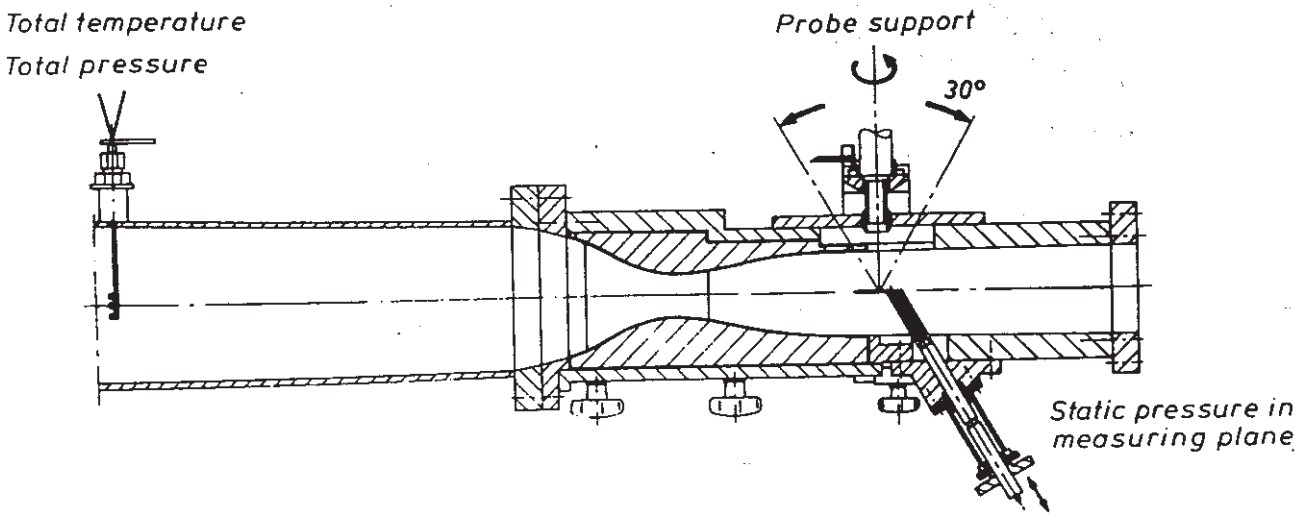


Fig. 2 Closed calibration tunnel (scheme)

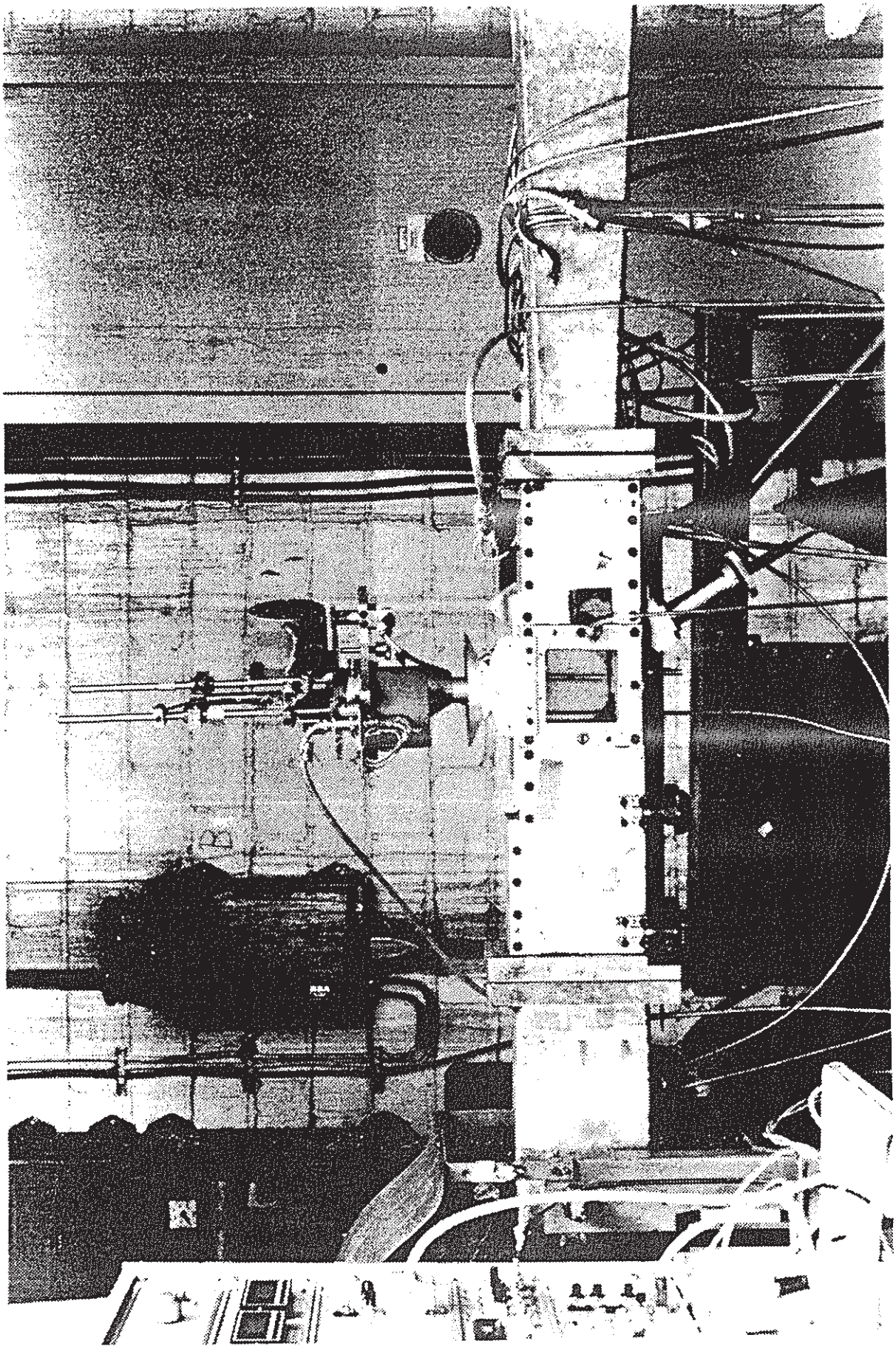

Fig. 3 Closed calibration tunnel with probe support

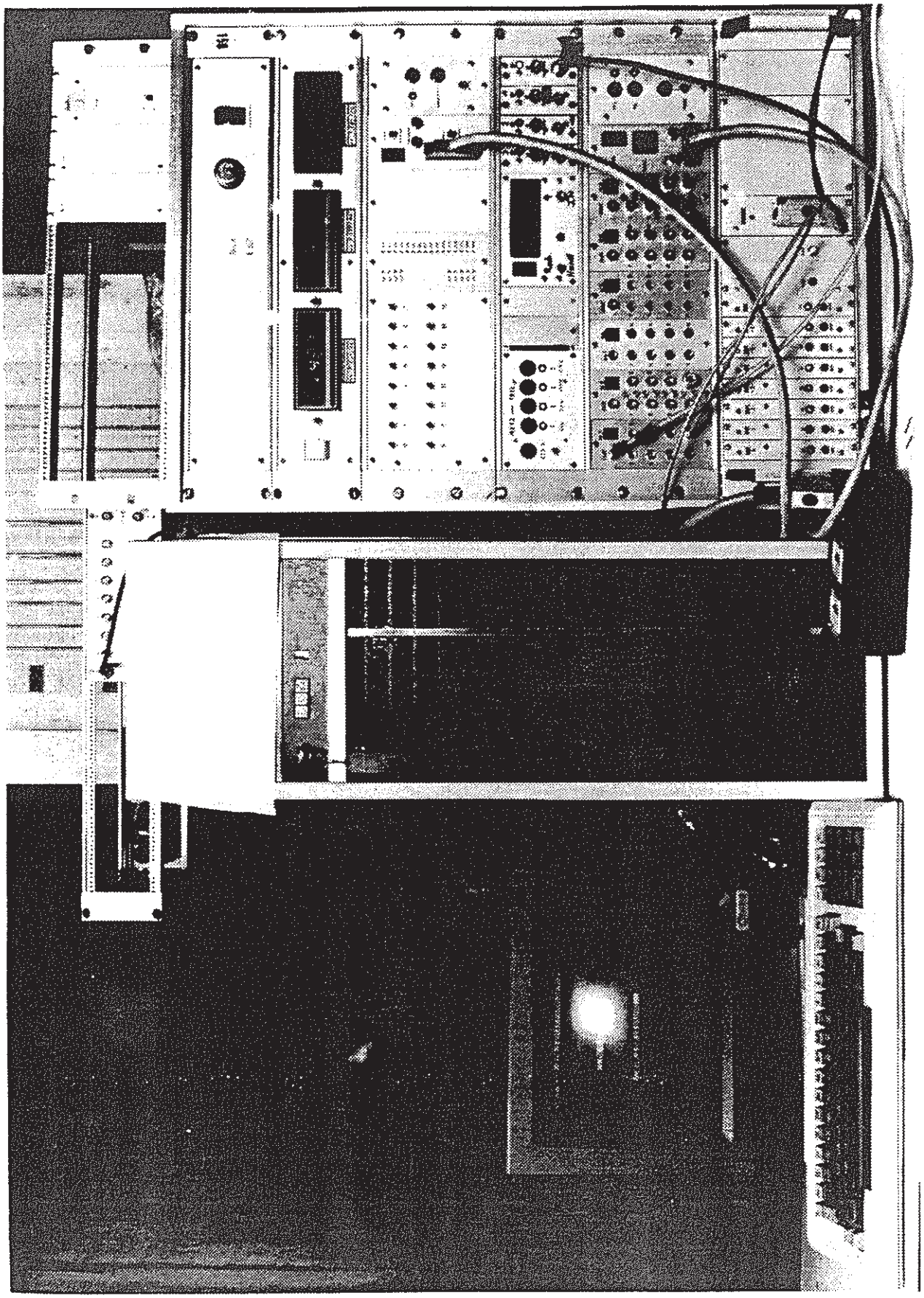

Fig. 4 Measuring equipment

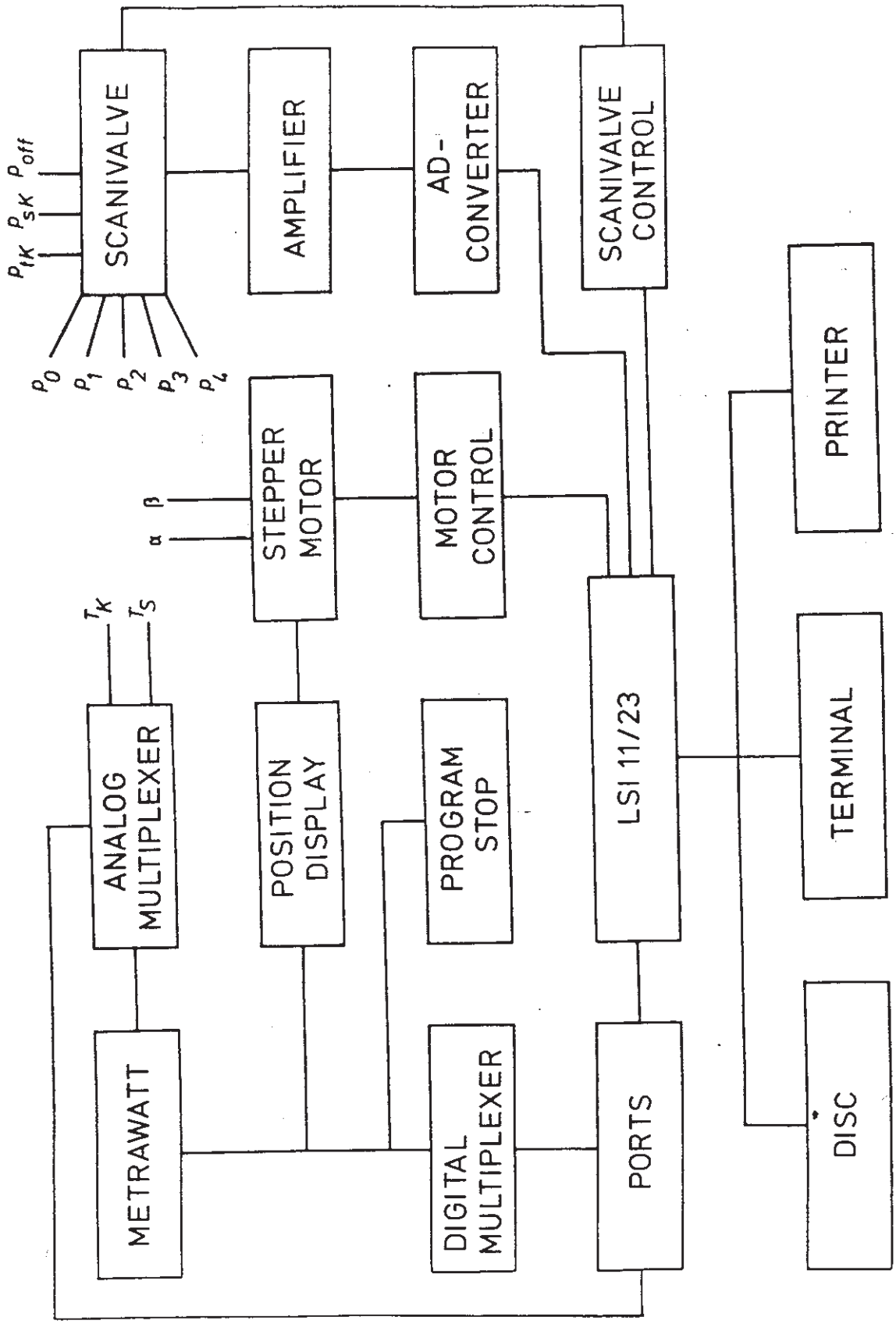


Fig. 5 Measuring connection scheme

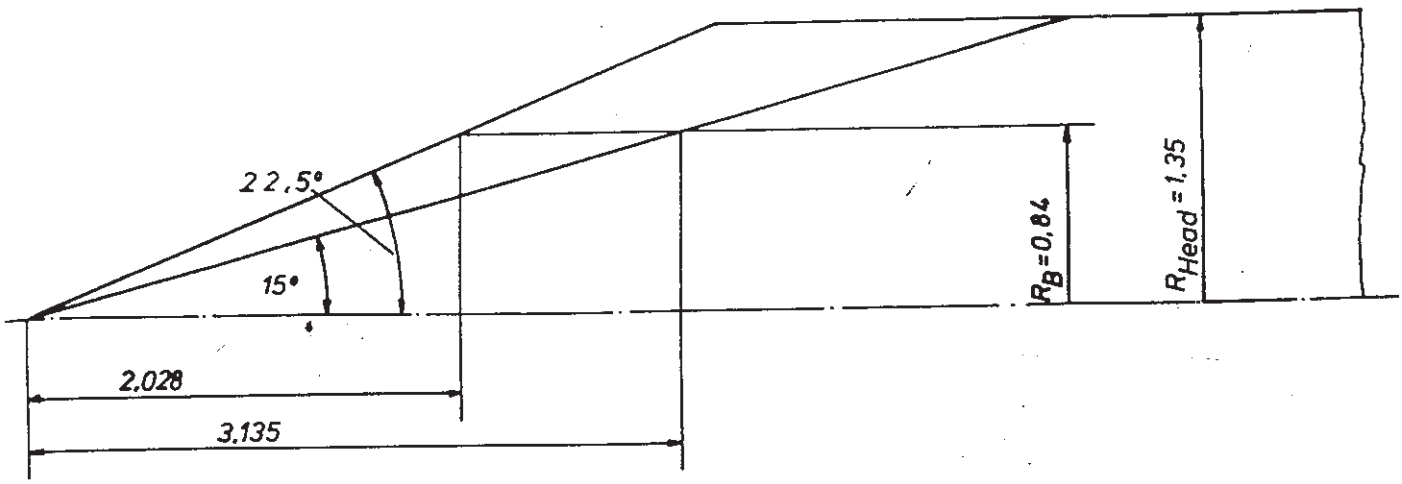


Fig. 6 Lateral bore holes

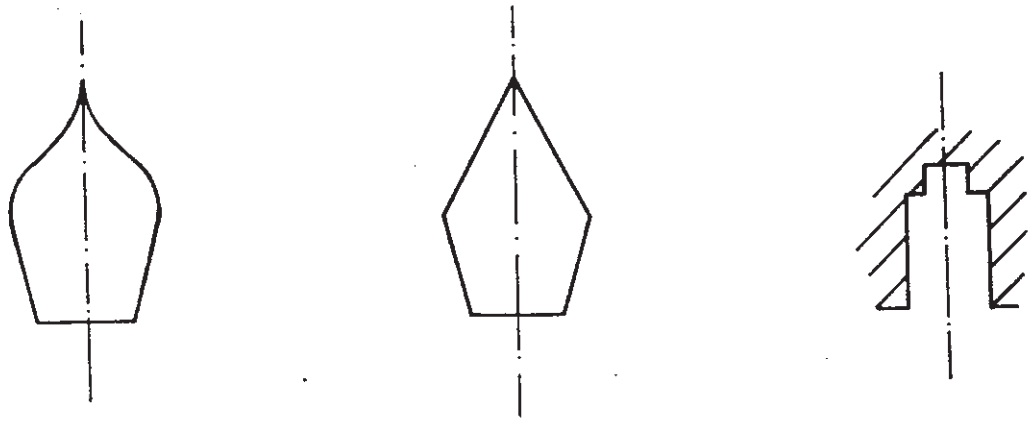

A: Drop

B: Rhombus

C: Space required for the pressure tubes

Fig. 7 Shaft cross-sections

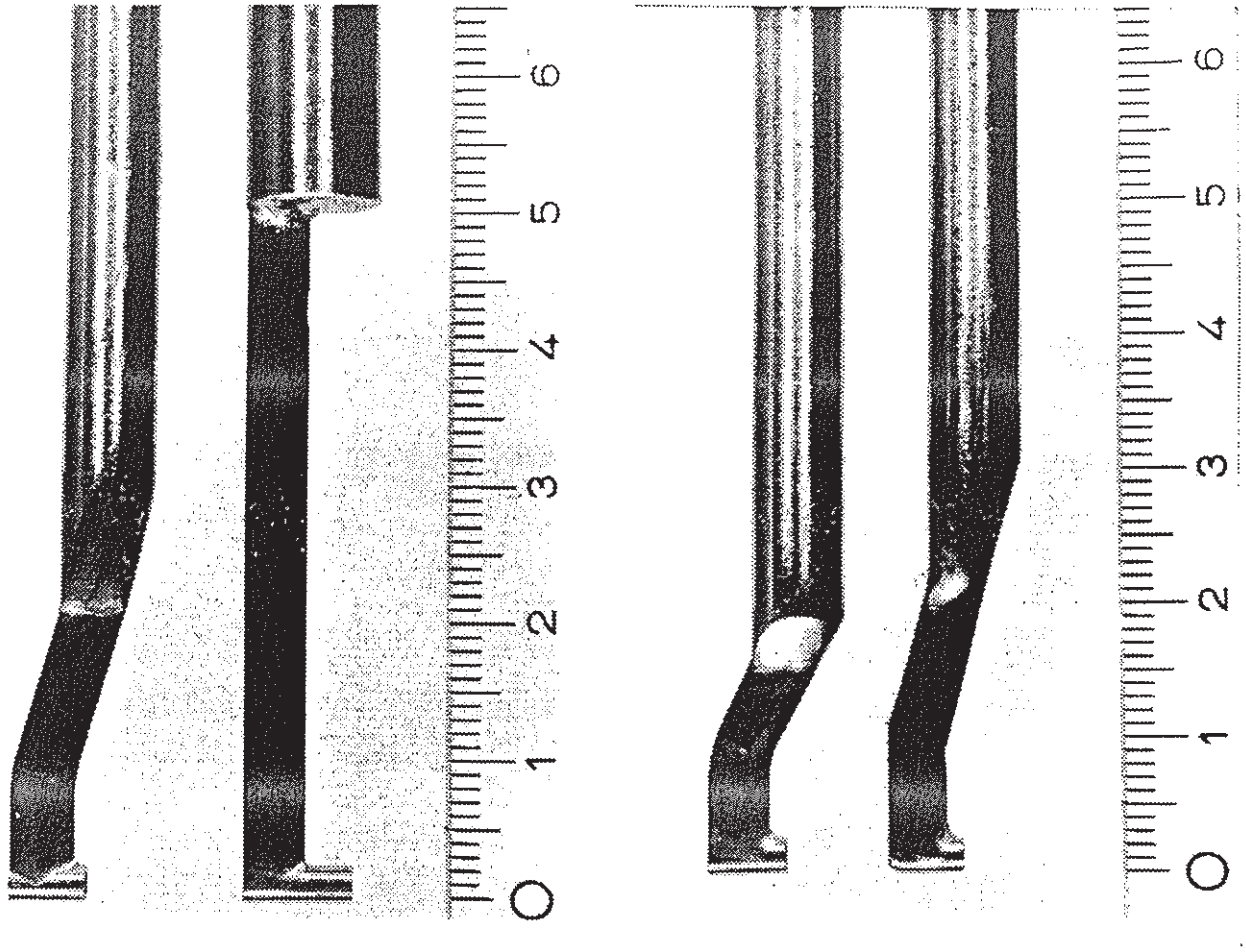


Fig. 8 Shaft dummies

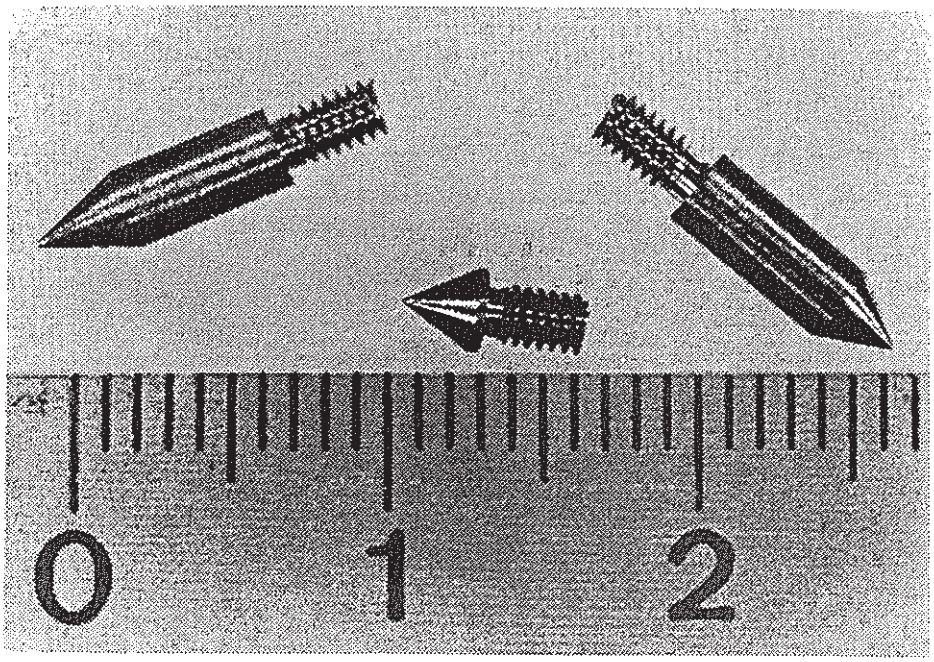


Fig. 9 Interchangeable dummy-heads

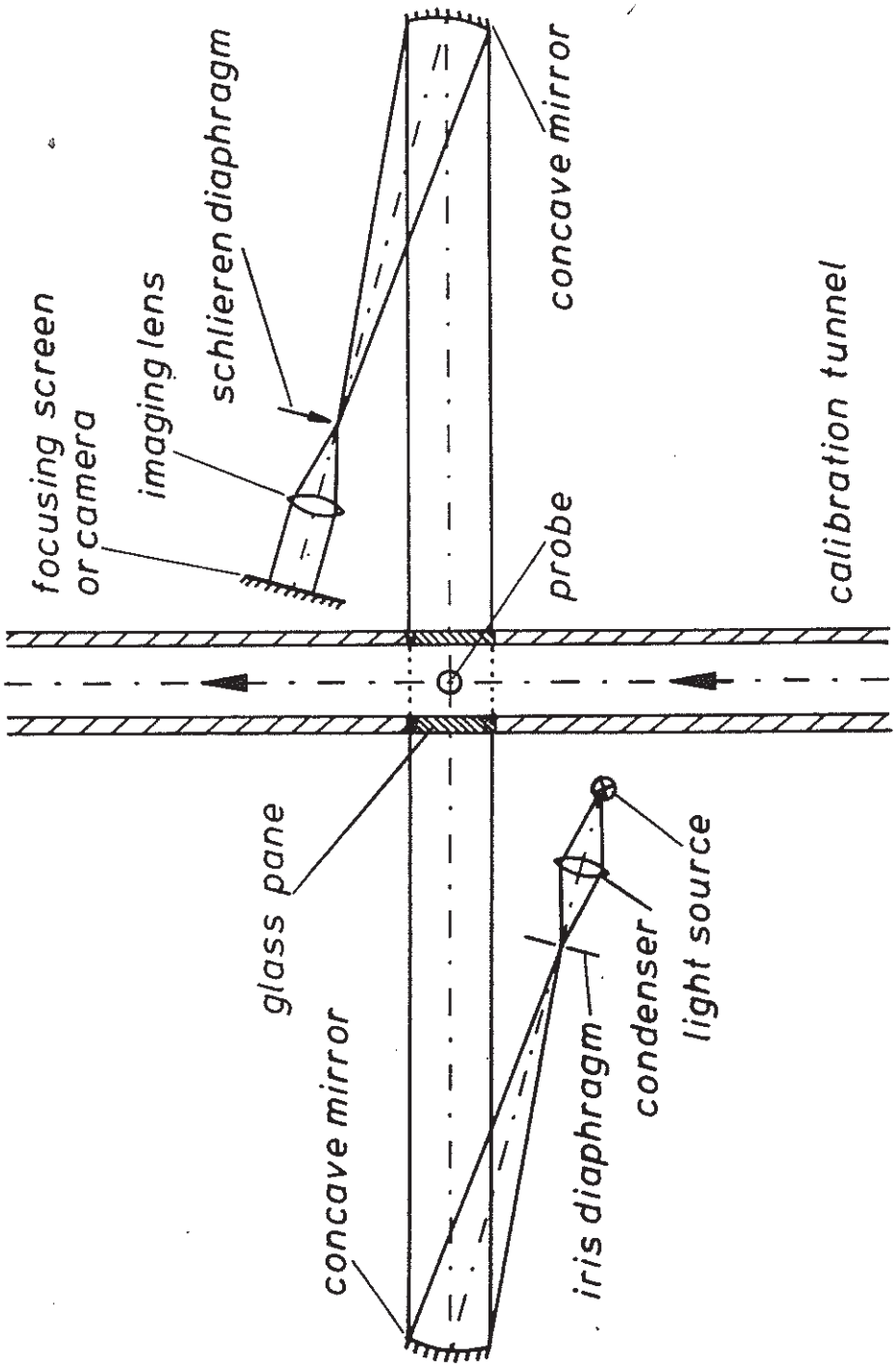


Fig. 10 Schlieren equipment

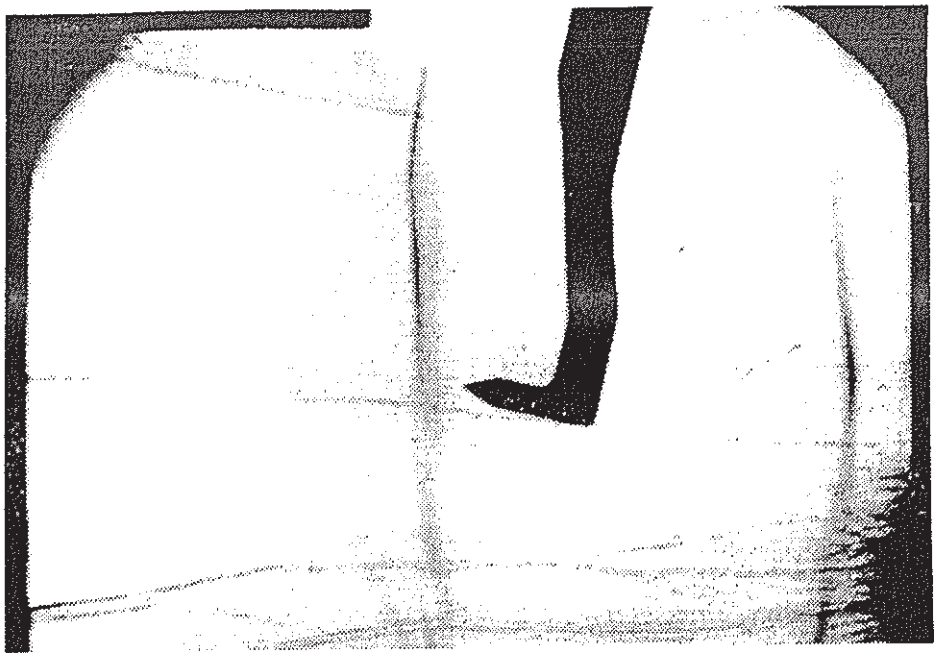

Fig. 11a Drop-design, large crimping, long head
$\delta = 45^0$, M = 1.17, $\alpha = 0^0$, $\beta = -15^0$

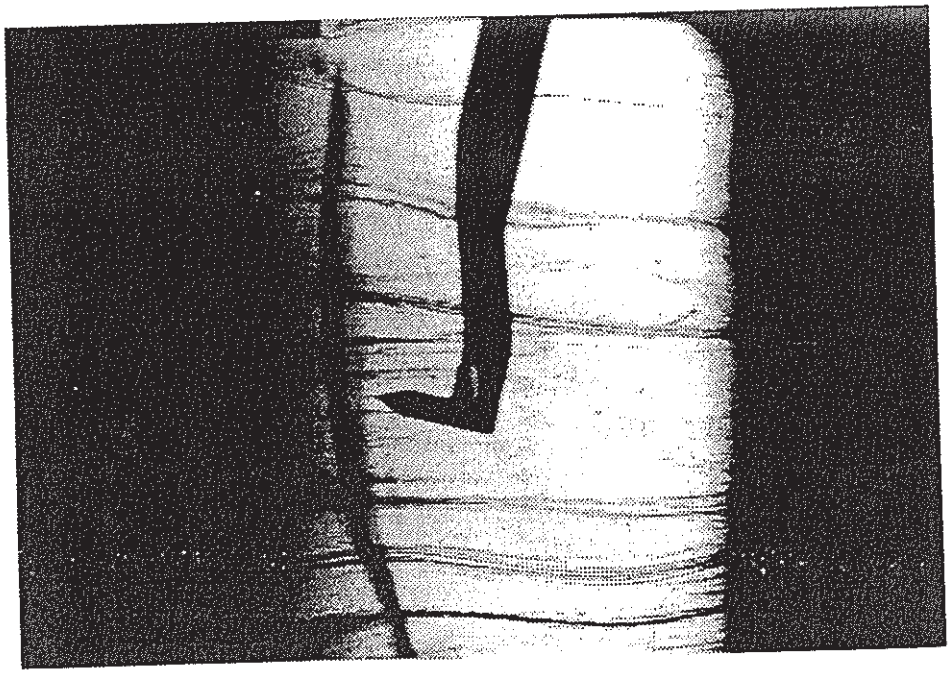

Fig. 11b Prismatic design, large crimping, long head
$\delta = 45^0$, M = 1.17, $\alpha = 0^0$, $\beta = -15^0$

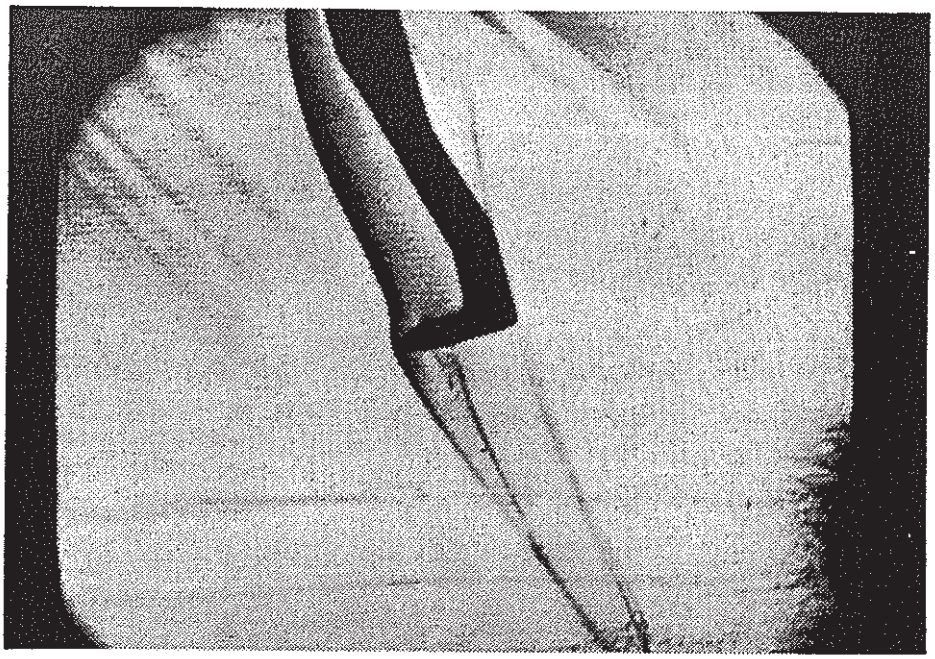

Fig. 11c Drop-design, large crimping, long head
$\delta = 45^0$, M = 1.4, $\alpha = 0^0$, $\beta = 15^0$

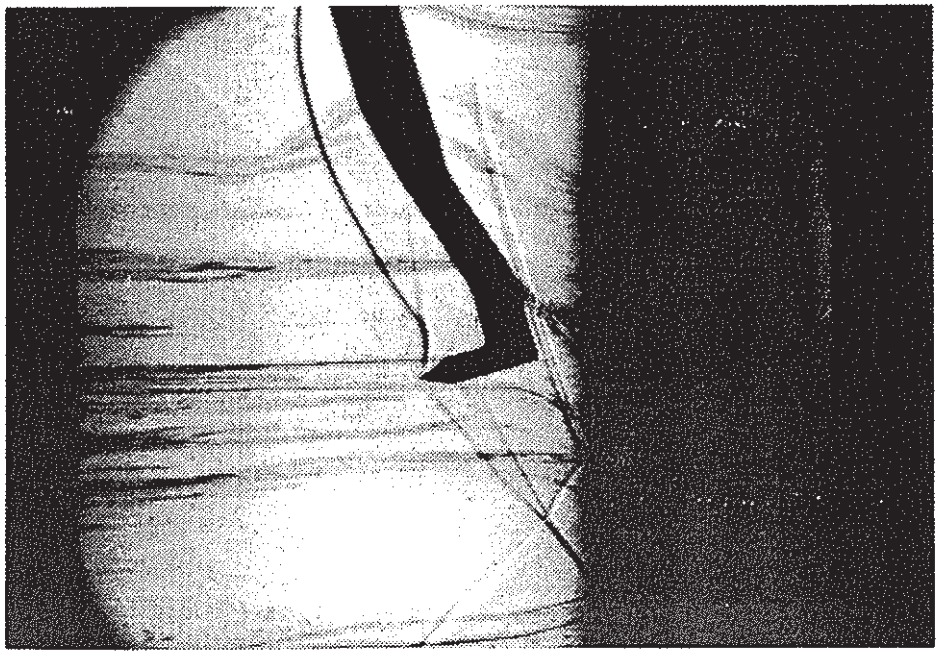

Fig. 11d Prismatic design, large crimping, long head
$\delta = 45^0$, M = 1.4, $\alpha = 0^0$, $\beta = 15^0$

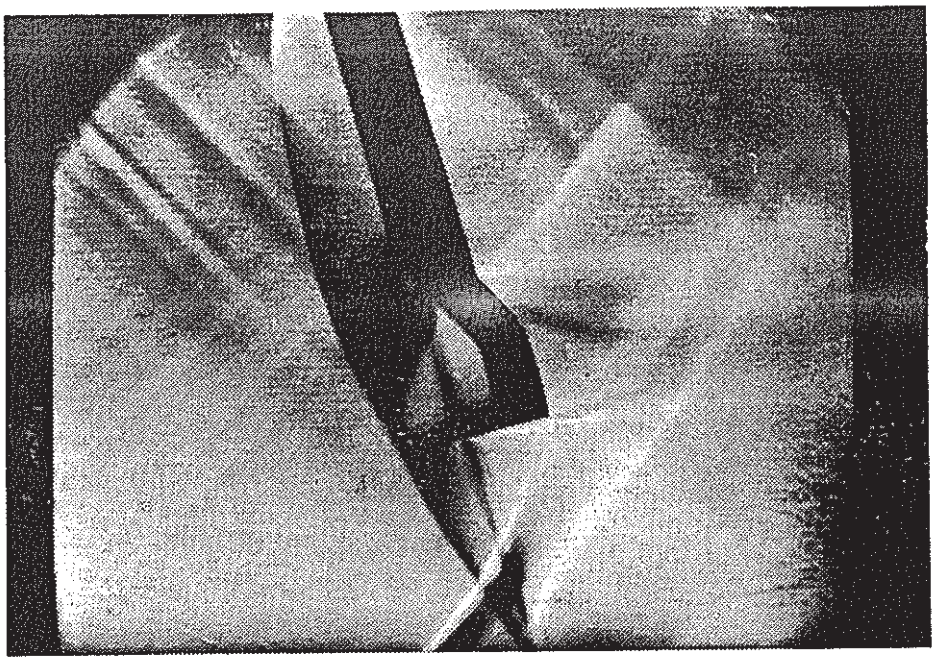

Fig. 12a Drop-design, small crimping, long head
$\delta = 45^0$, M = 1.4, $\alpha = 0^0$, $\beta = 15^0$

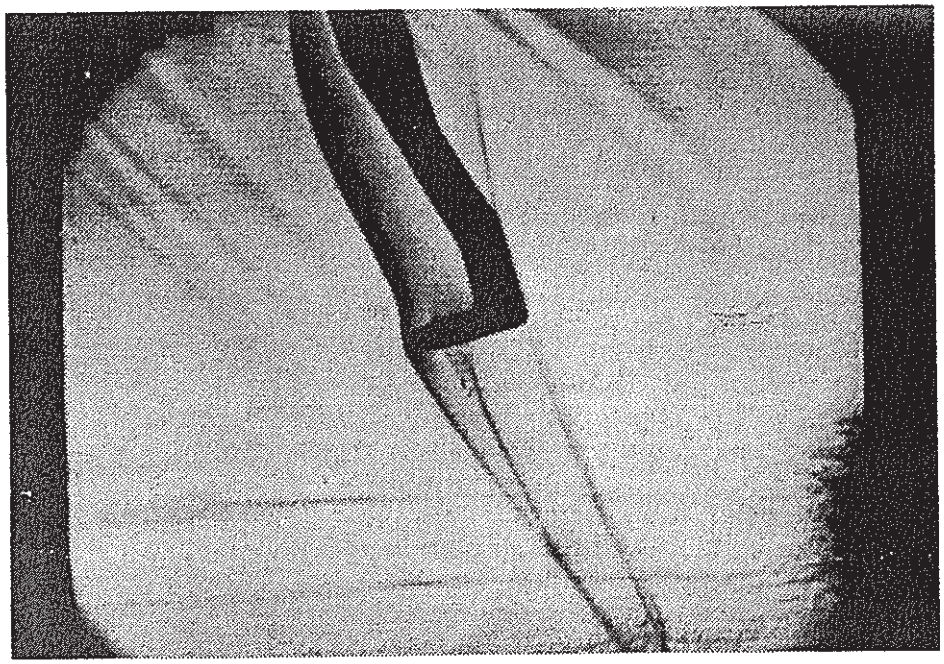

Fig. 12b Drop-design, large crimping, long head
$\delta = 45^0$, M = 1.4, $\alpha = 0^0$, $\beta = 15^0$

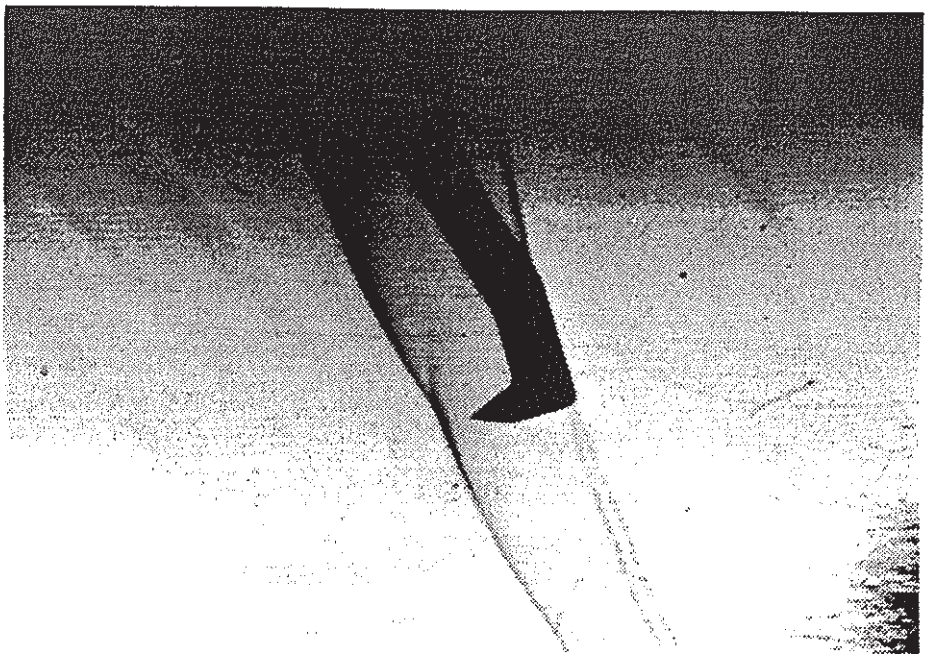

Fig. 13a Drop-design, large crimping, short head
$\delta = 45^0$, M = 1.4, $\alpha = 0^0$, $\beta = 15^0$

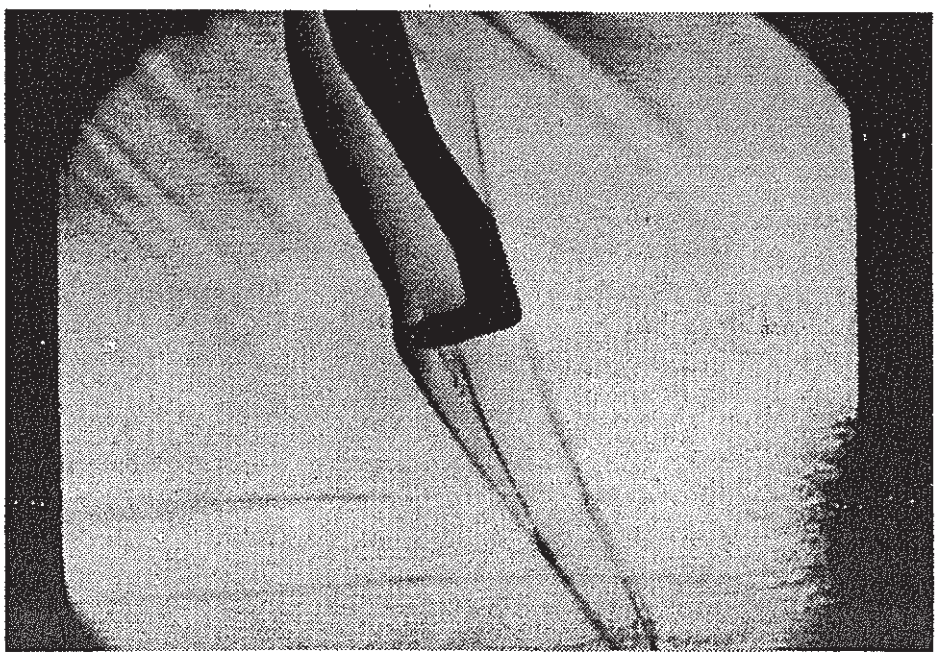

Fig. 13b Drop-design, large crimping, long head
$\delta = 45^0$, M = 1.4, $\alpha = 0^0$, $\beta = 15^0$

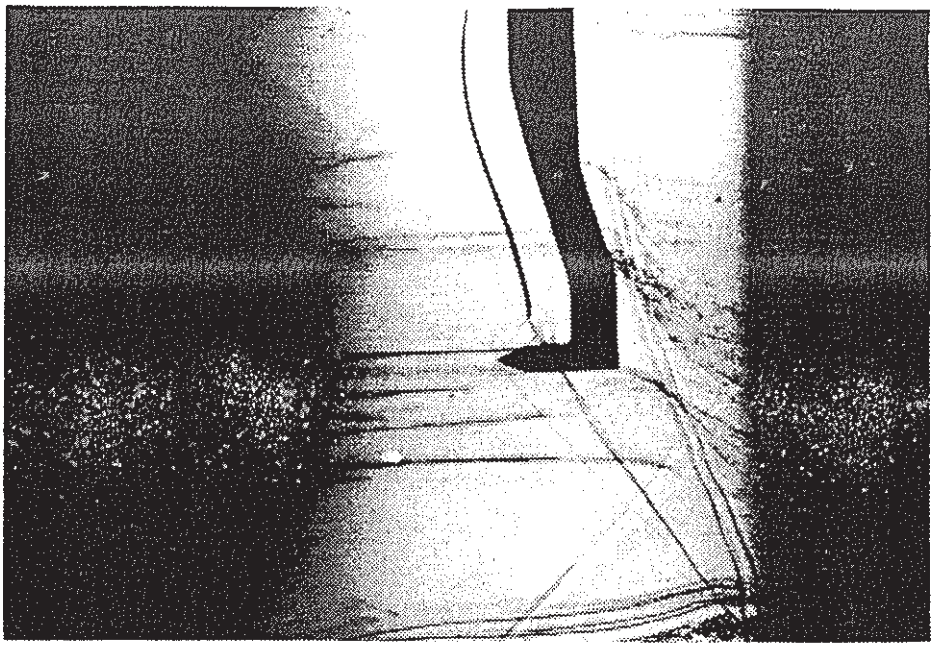

Fig. 14a Prismatic design, large crimping, long head
$\delta = 45^0$, M = 1.4, $\alpha = 0^0$, $\beta = 0^0$

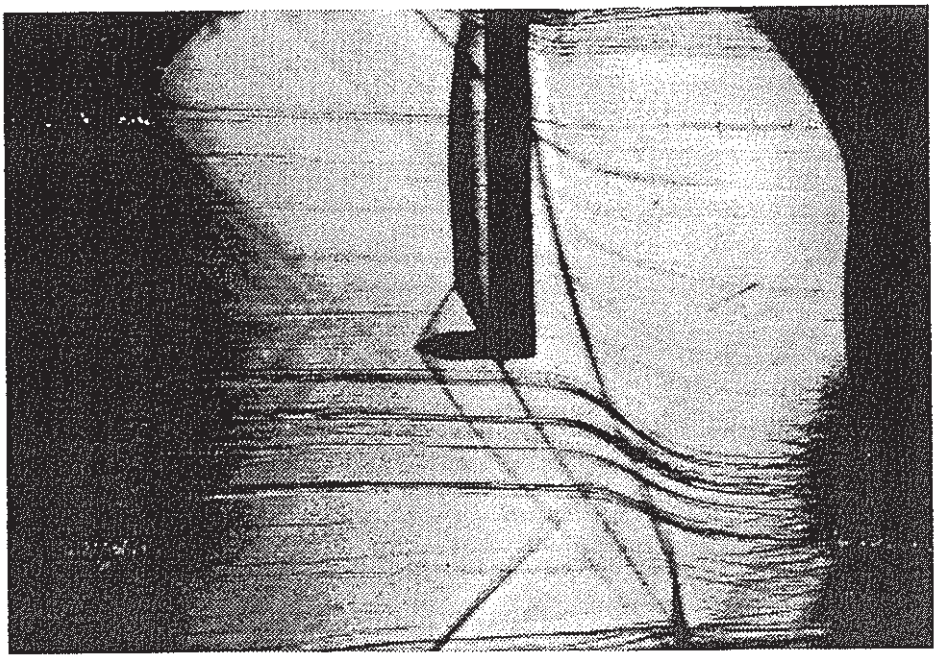

Fig. 14b Prismatic design, straight shaft, long head
$\delta = 45^0$, M = 1.4, $\alpha = 0^0$, $\beta = 0^0$

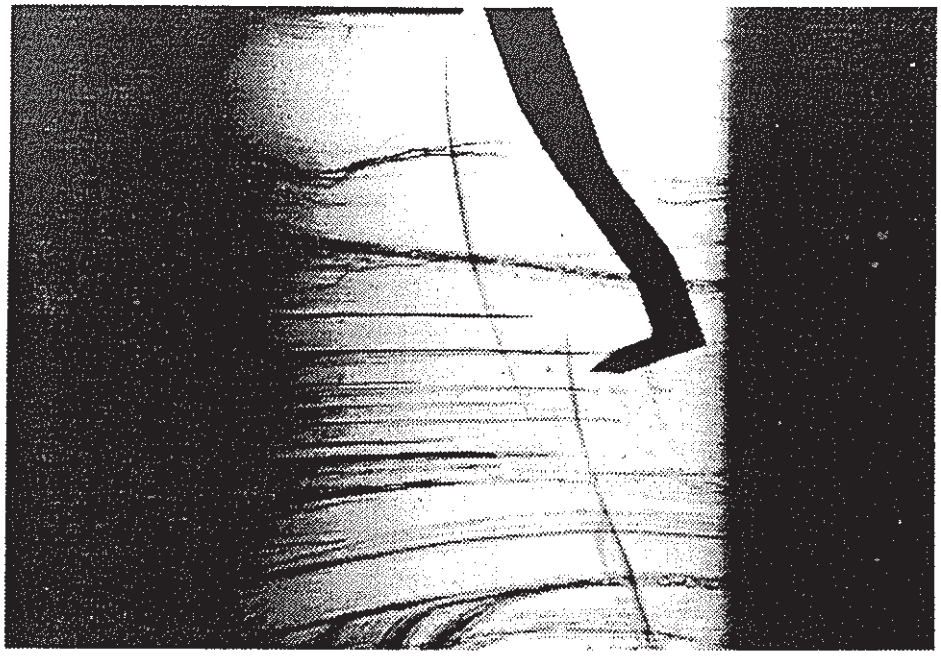

Fig. 15a Prismatic design, large crimping, long head
$\delta = 45^{0}$, M = 1.17, $\alpha = 0^{0}$, $\beta = 15^{0}$

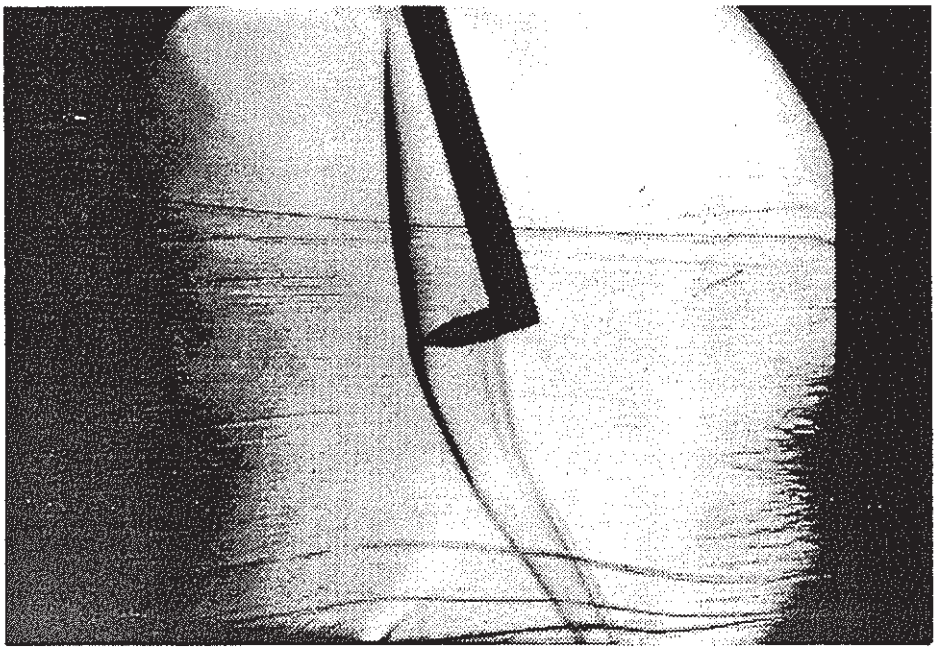

Fig. 15b Prismatic design, straight shaft, long head
$\delta = 45^{0}$, M = 1.17, $\alpha = 0^{0}$, $\beta = 15^{0}$

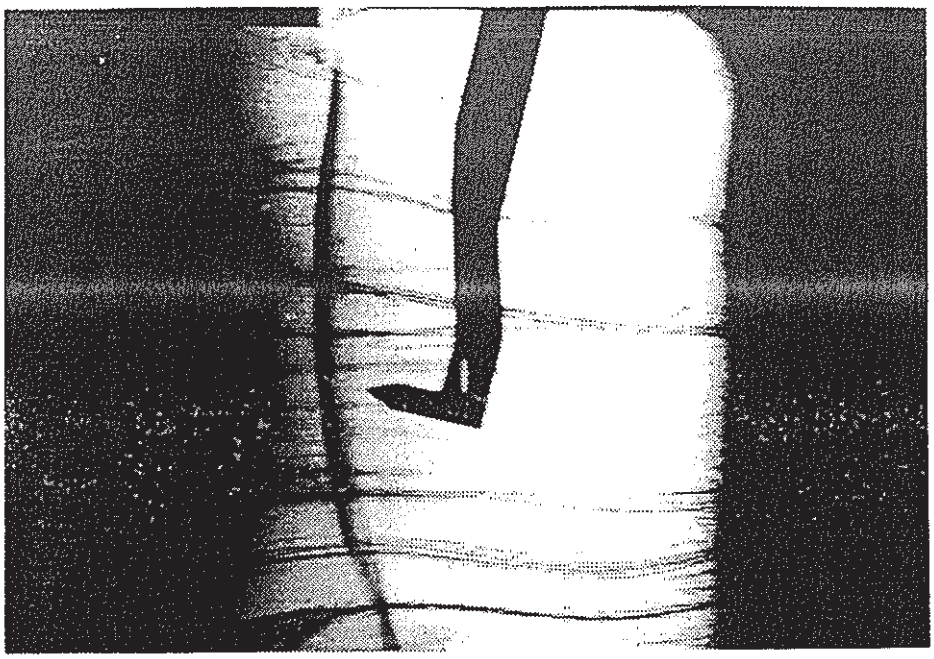

Fig. 15c Prismatic design, large crimping, long head
$\delta = 45^0$, M = 1.17, $\alpha = 0^0$, $\beta = -15^0$

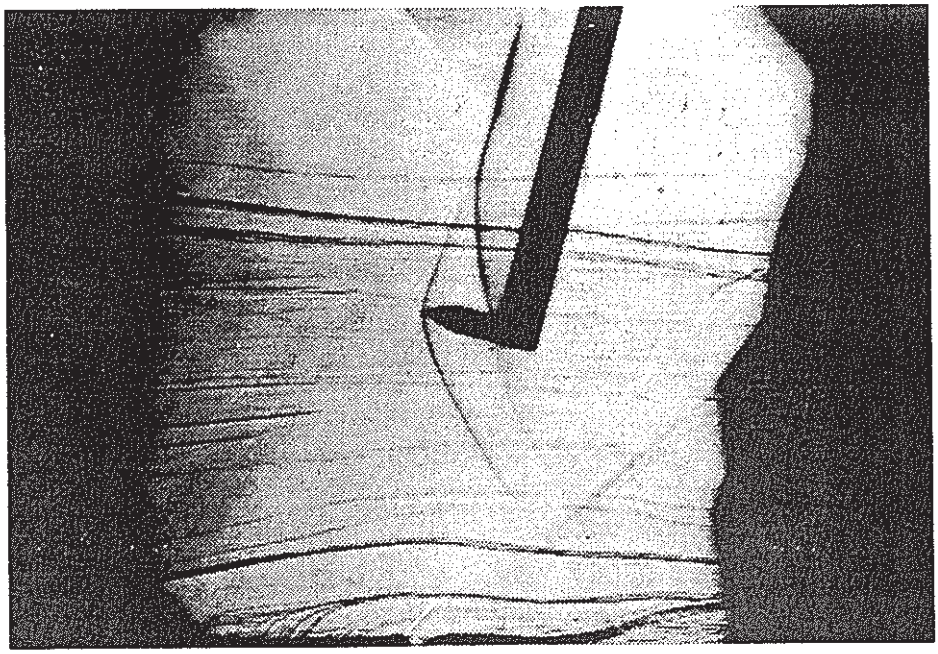

Fig. 15d Prismatic design, straight shaft, long head
$\delta = 45^0$, M = 1.17, $\alpha = 0^0$, $\beta = -15^0$

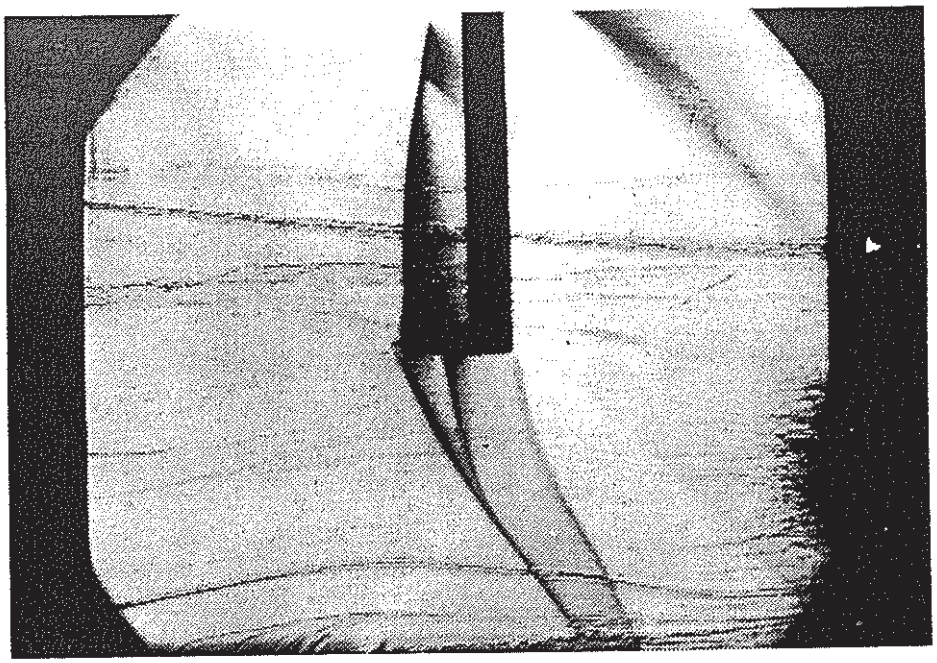

Fig. 16a Prismatic design, straight shaft, long head
$\delta = 30^0$, M = 1.17, $\alpha = 0^0$, $\beta = 0^0$

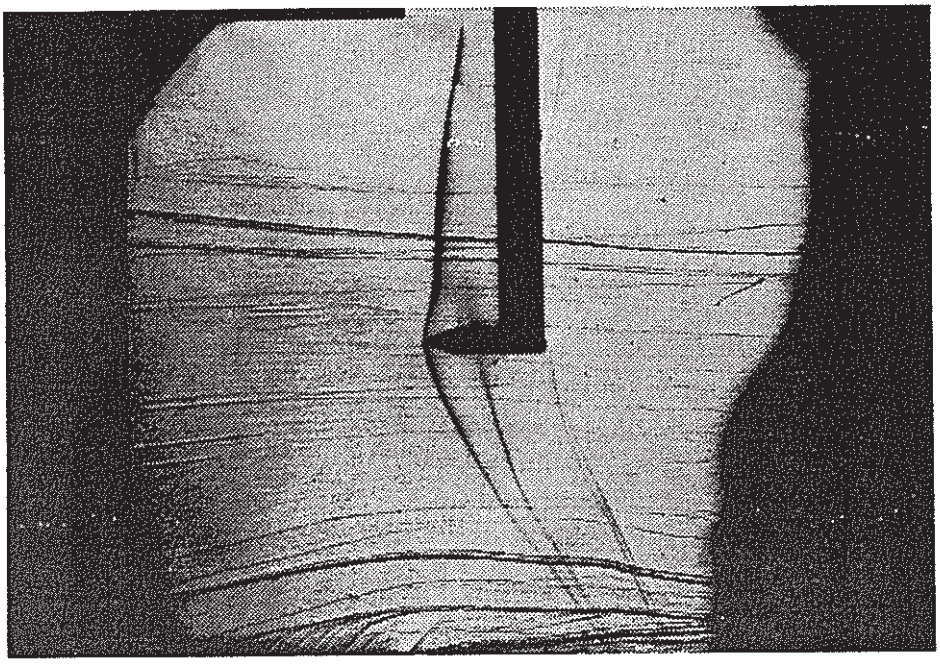

Fig. 16b Prismatic design, straight shaft, long head
$\delta = 45^0$, M = 1.17, $\alpha = 0^0$, $\beta = 0^0$

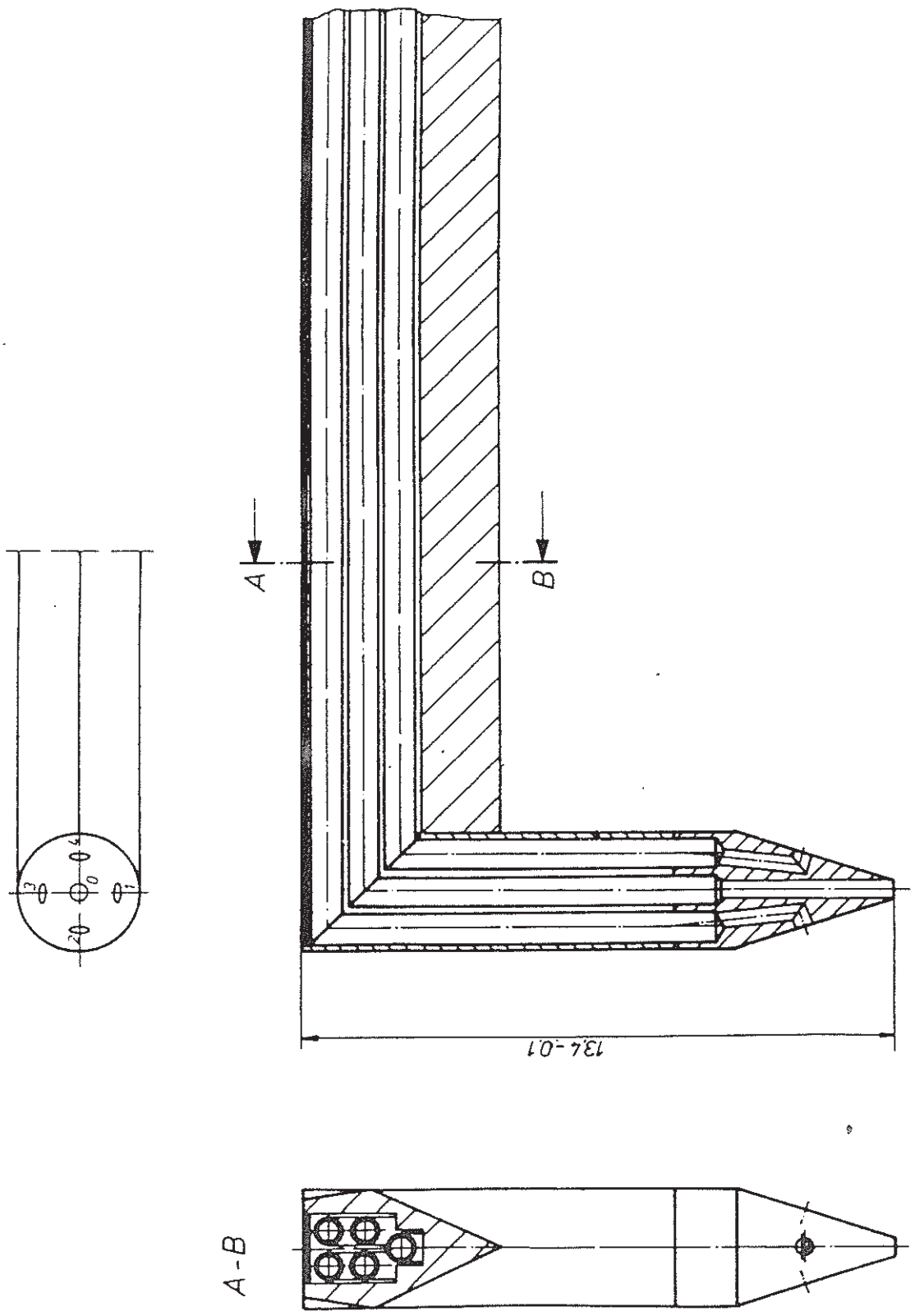


Fig. 17 Final probe construction

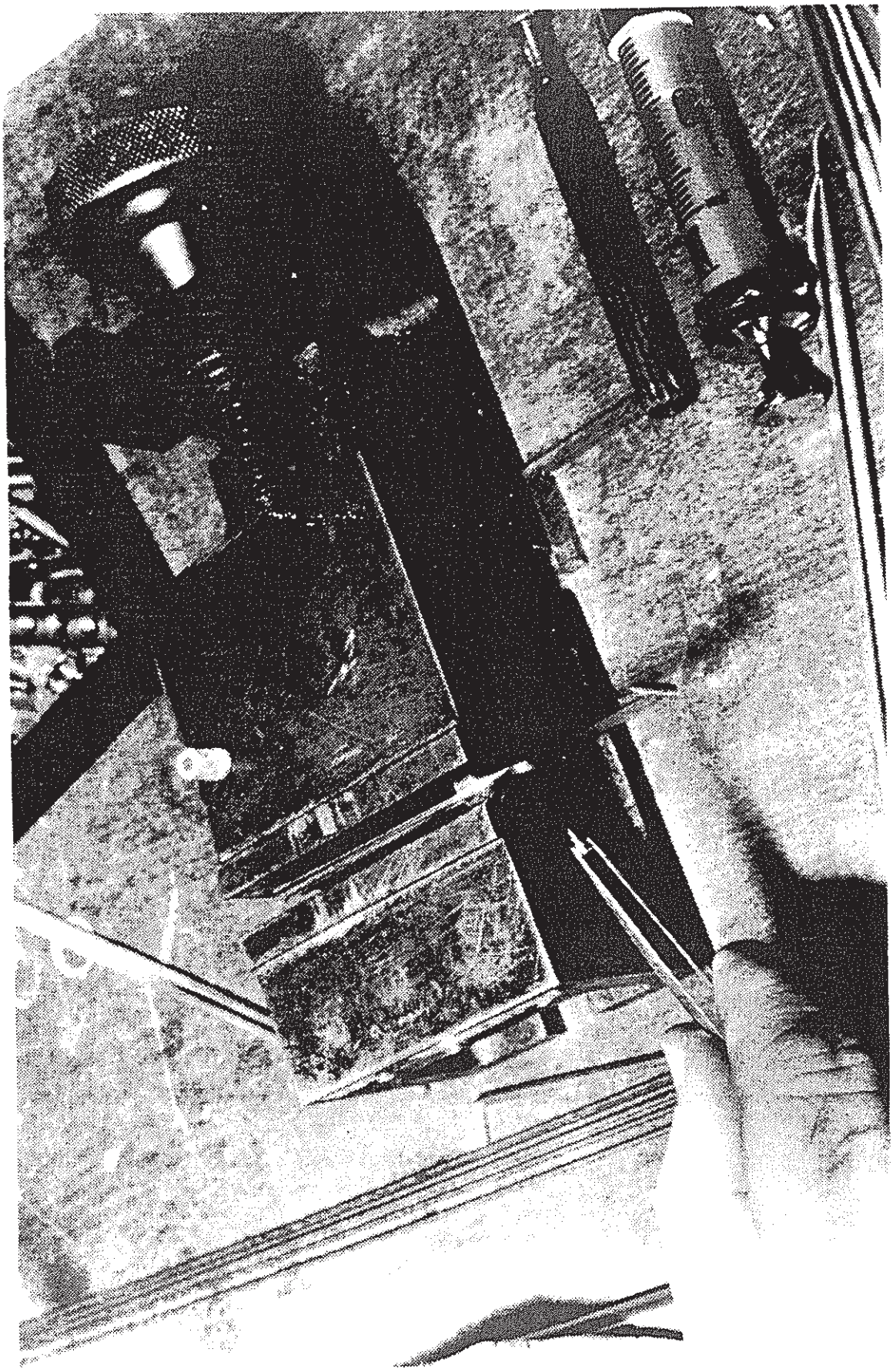

Fig. 18 Probe workshop

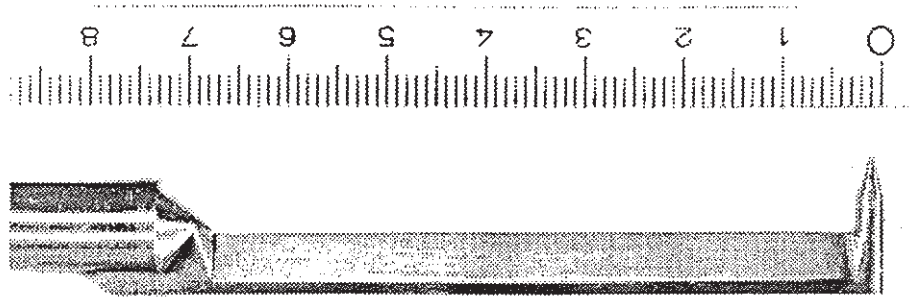


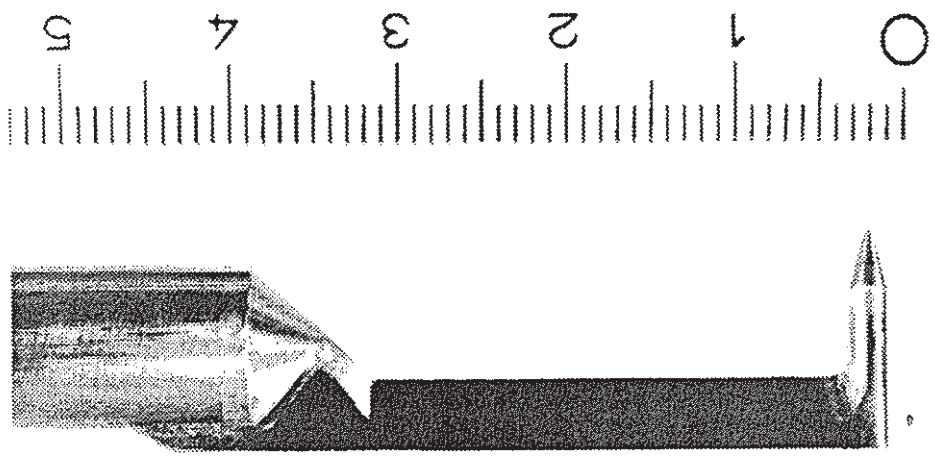


Fig. 19 Five-hole probe with two shaft-variants

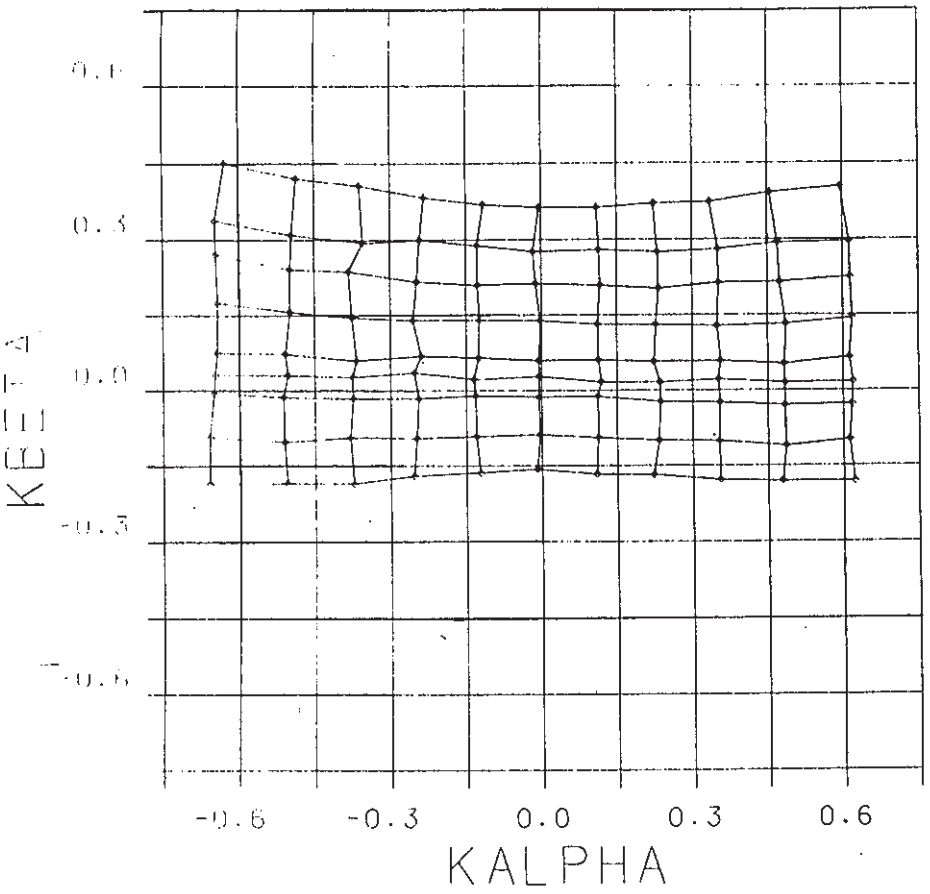


SONDE 935/1
EICHDATUM 26.10.87
MACHZAHL ◇0.50

Fig. 20 Calibration map for a subsonic Mach number

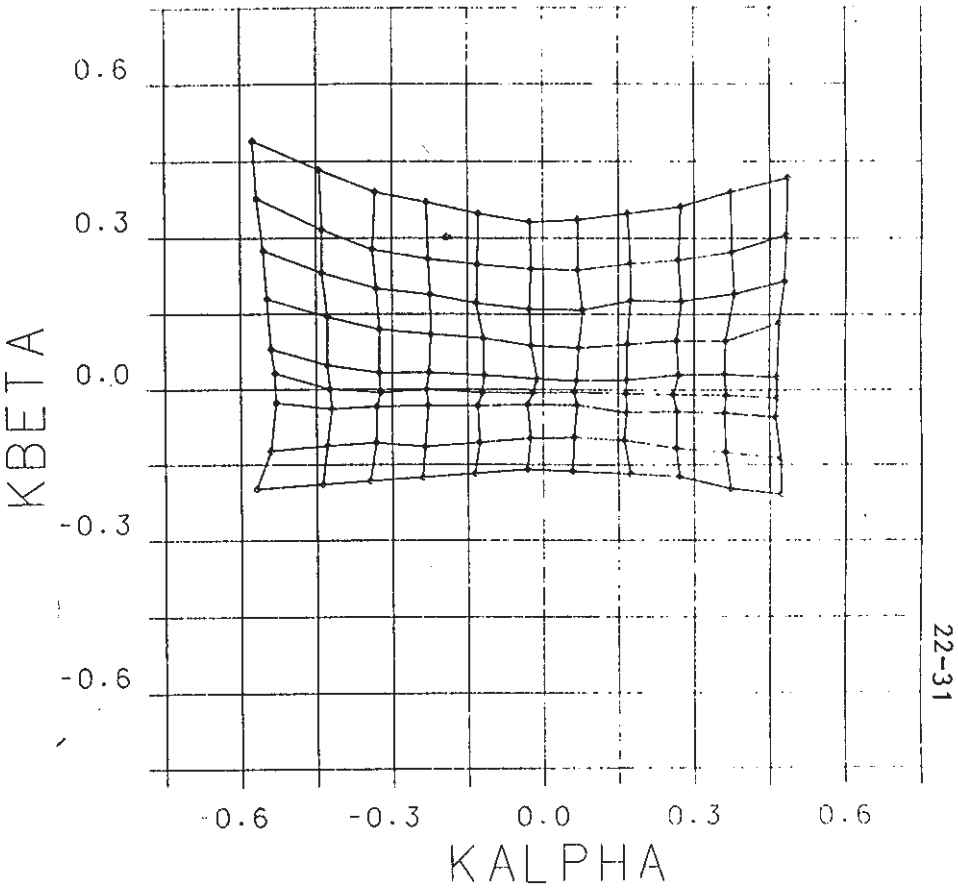


SONDE 935/1
EICHDATUM 26.10.87
MACHZAHL ◇1.21

Fig. 21 Calibration map for a supersonic Mach number

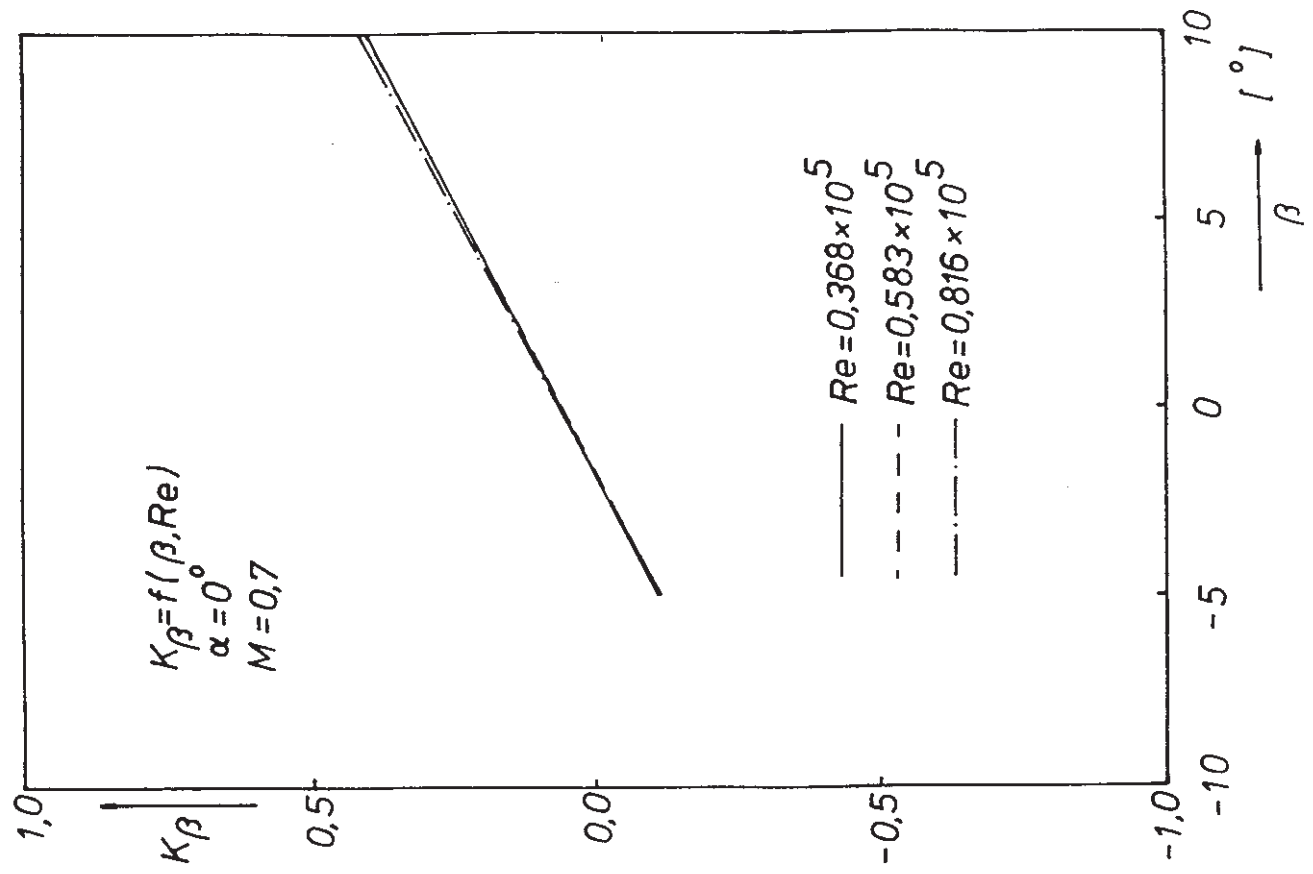
$K_\beta = f(\beta, Re)$
$\alpha = 0^\circ$
$M = 0,7$
$K_\beta$
1,0
0,5
0,0
-0,5
-1,0
10
5
0
-5
-10
$\beta$ [°]
$Re = 0,368 \times 10^5$
$Re = 0,583 \times 10^5$
$Re = 0,816 \times 10^5$

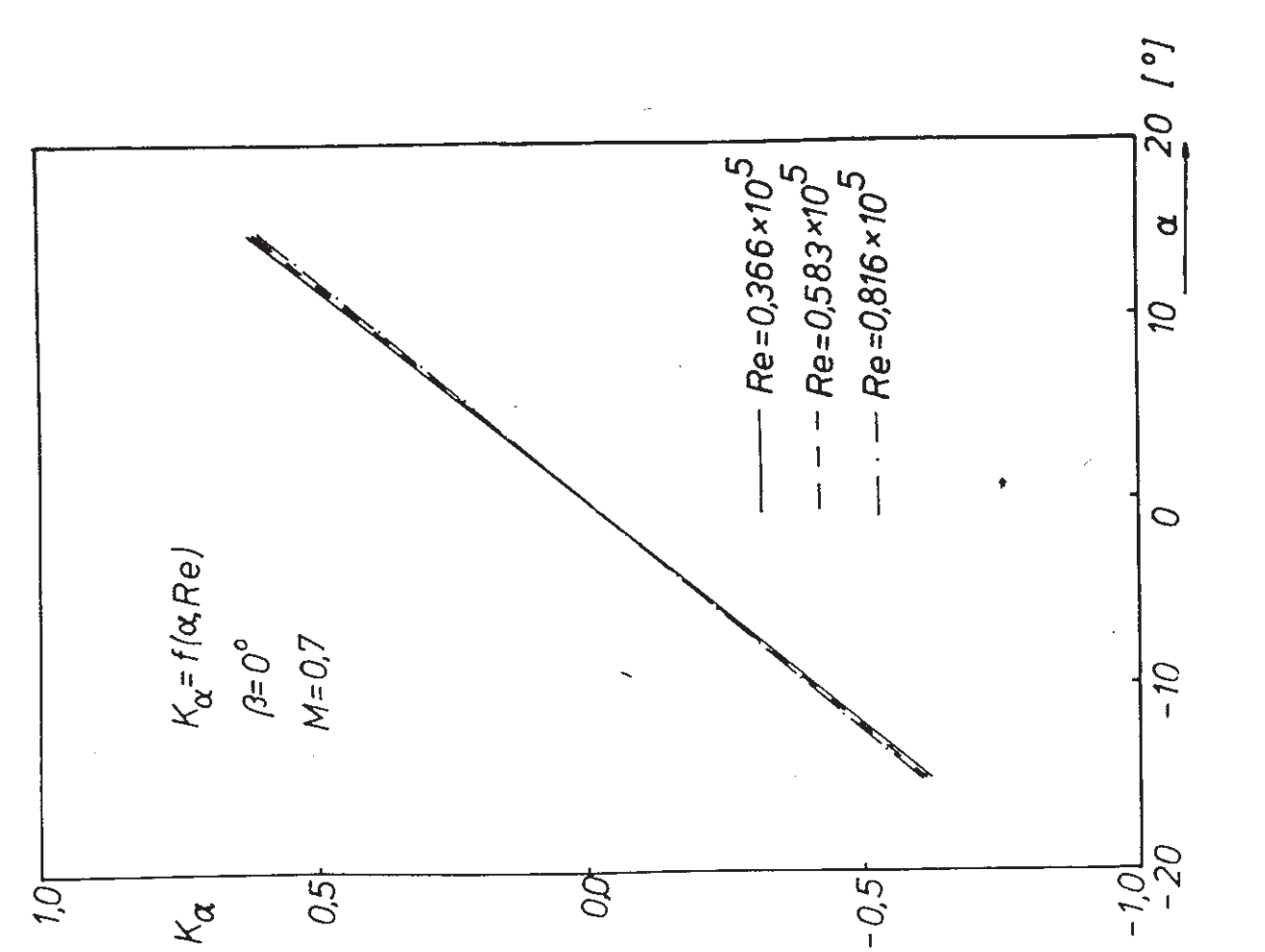
$K_\alpha = f(\alpha, Re)$
$\beta = 0^\circ$
$M = 0,7$
$K_\alpha$
1,0
0,5
0,0
-0,5
-1,0
20
10
0
-10
-20
$\alpha$ [°]
$Re = 0,366 \times 10^5$
$Re = 0,583 \times 10^5$
$Re = 0,816 \times 10^5$

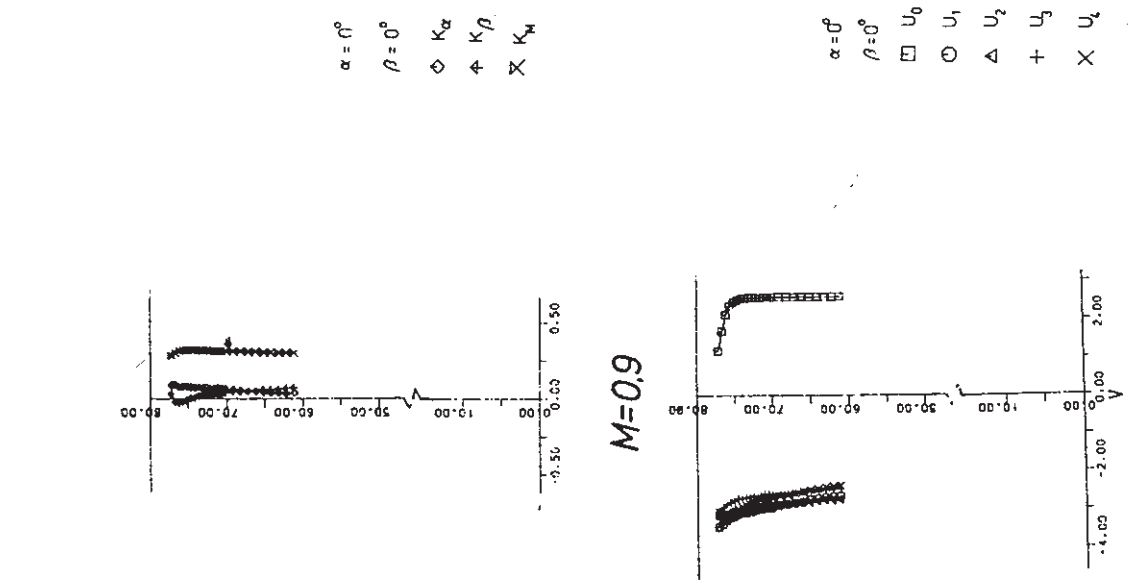


Fig. 23b Wall influence
(subsonic, upper wall)

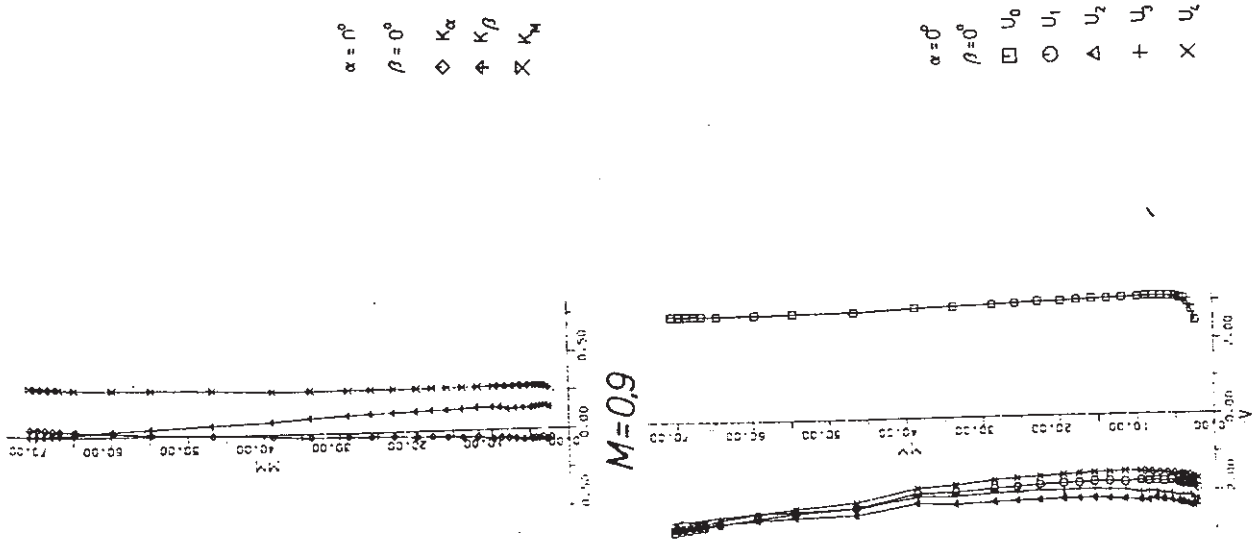


Fig. 23a Wall influence
(subsonic, lower wall)

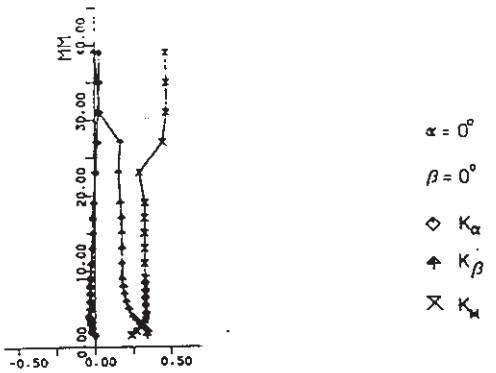


M=1,33

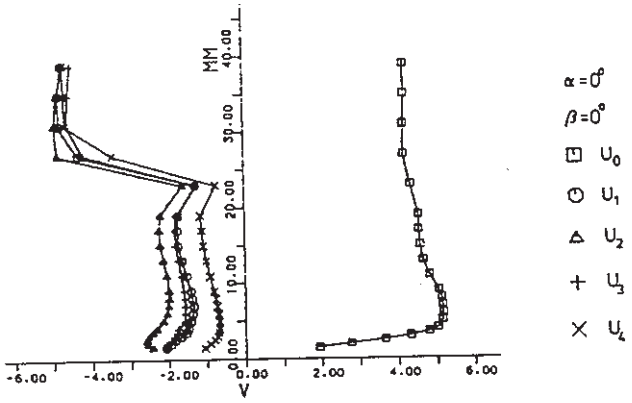


Fig. 23c Wall influence
(supersonic, lower wall)